Combustion, Explosion, and Shock Waves, Vol. 41, No. 6, pp. 657–679, 2005

Thermal Decomposition and Combustion of Ammonium Dinitramide (Review)

R. Yang,[1] P. Thakre,[2] and V. Yang[2]

UDC 536.46

Translated from *Fizika Goreniya i Vzryva*, Vol. 41, No. 6, pp. 54–79, November–December, 2005.
Original article submitted May 12, 2005.

A comprehensive review of thermal decomposition and combustion of ammonium dinitramide (ADN) has been conducted. The basic thermal properties, chemical pathways, and reaction products in both the condensed and gas phases are analyzed over a broad range of ambient conditions. Detailed combustion-wave structures and burning-rate characteristics are discussed. Prominent features of ADN combustion are identified and compared with other types of energetic materials. In particular, the influence of various condensed- and gas-phase processes in dictating the pressure and temperature sensitivities of the burning rate is examined. In the condensed phase, decomposition proceeds through the mechanisms ADN → $NH_4NO_3 + N_2O$ and ADN → $NH_3 + HNO_3 + N_2O$, the former mechanism being the basic one. In the gas phase, the mechanisms ADN → NH_3 + HDN and ADN → $NH_3 + HNO_3 + N_2O$ are prevalent. The gas-phase combustion-wave structure in the range of 5–20 atm consists of a near-surface primary flame followed by a dark-zone temperature plateau at 600–1000°C and a secondary flame followed by another dark-zone temperature plateau at 1000–1400°C. At higher pressures (60 atm and above), a final flame is observed at about 1800°C without the existence of any dark-zone temperature plateau. ADN combustion is stable in the range of 5–20 atm and the pressure sensitivity of the burning rate has the form $r_b = 20.72p^{0.604}$ [mm/sec] ($p = 0.5$–2.0 MPa). The burning characteristics are controlled by exothermic decomposition in the condensed phase. Above 100 atm, the burning rate is well correlated with pressure as $r_b = 8.50p^{0.608}$ [mm/sec] ($p = 10$–36 MPa). Combustion is stable, and intensive heat feedback from the gas phase dictates the burning rate. The pressure dependence of the burning rate, however, becomes irregular in the range of 20–100 atm. This phenomenon may be attributed to the competing influence of the condensed-phase and gas-phase exothermic reactions in determining the propellant surface conditions and the associated burning rate.

Key words: energetic materials, ammonium dinitramide (ADN), thermal decomposition, combustion mechanism.

INTRODUCTION

The inorganic oxidizer ammonium dinitramide (ADN) is considered to be a viable and ecologically preferable alternative to ammonium perchlorate (AP) in solid propellants because of its high burning rate and chlorine-free combustion products. Hence, ADN has attracted substantial attention in the energetic materials community [1–3]. The chemical formula of ADN is $NH_4^+N(NO_2)_2^-$, which essentially represents an ammonium salt of dinitramic acid $HN(NO_2)_2$, referred to as HDN. To date, along with ADN and KDN [potassium dinitramide, $KN(NO_2)_2$], more than eighty different kinds of organic and inorganic amines, metal salts, and complex salts of dinitramide have been developed [3–10].

---

[1] School of Materials Science and Engineering, Beijing Institute of Technology, Beijing 100081, China.

[2] Department of Mechanical and Nuclear Engineering, The Pennsylvania State University, PA 16801, USA; vigor@psu.edu.

A study of ADN properties published by Russian scientists [11] in 1993 stated its X-ray density as 1.82–1.84 g/cm^3, enthalpy of formation $\Delta H_f^0(298\ K) = -256.3$ kcal/kg, and melting point as 92.5°C. The crystal density of ADN was recently reported to be 1.8 g/cm^3 [12]. The enthalpy of formation and the X-ray density of ADN reported by American scientists [13] are −35.8 kcal/mole (−288.70 kcal/kg) and 1.801 g/cm^3 (ADN purity 99%), respectively. The melting point of the ADN crystal is usually 92–95°C and varies with the amount of the ammonium nitrate (AN) impurity present [14]. The higher the AN impurity, the lower the melting point; it is typically 55°C for an ADN/AN (70/30 mole fraction) eutectic [15].

ADN is known to exist in two polymorphic forms: α-ADN and β-ADN [14]. For $p < 2 \cdot 10^4$ atm, α-ADN with a stable monoclinic prism crystal structure is observed, and β-ADN exists only at higher pressures ($p > 2 \cdot 10^4$ atm). Ultraviolet (UV) characteristic bands of ADN in an aqueous solution are similar to those of ammonium nitrate, sodium nitrite ($NaNO_2$), and cyclotetramethylenetetranitramine (HMX) [2, 16, 17] in the wavelength ranges of 220–250 nm and 280–300 nm. Infrared and Raman spectra of ADN and other dinitramide salts reported by Shlyapochnikov et al. [17–19] and Christe et al. [20] show strong IR absorptions at 1526 cm^{-1} (asymmetric stretch of NO_2 in phase), 1181 cm^{-1} (symmetric stretch of NO_2 out of phase), 1025 cm^{-1} (asymmetric stretch of N_3), and 3255 cm^{-1} (NH_4^+) and 1407 cm^{-1} (NH_4^+). The large energy release in ADN combustion ($\Delta H_f = -35.8$ kcal/mole) as compared to AN ($\Delta H_f = -78$ kcal/mole) and AP ($\Delta H_f = -70.7$ kcal/mole) is attributed to the higher heat of formation of ADN [21]. The similarity in the chemical structures of ADN and AN allows comparative studies between these two compounds [21], since their thermal decomposition and combustion characteristics are closely related.

Significant experimental and theoretical efforts have been applied to study physicochemical properties, thermal decomposition [21–38] and combustion mechanisms [30–33] of ADN. The experimental techniques employed include differential scanning calorimetry (DSC), thermal gravimetric analysis (TGA), differential thermal analysis (DTA), microprobe mass spectroscopy (MS), Fourier transition infrared spectroscopy (FTIR), ^{15}N isotopic analysis, and combined MS/FTIR. The combustion characteristics of ADN have been studied by conducting measurements of temperature profiles [12], burning rates in constant-pressure reservoirs [12, 31, 34], and species concentrations [24], as well as by theoretical and numerical modeling [32, 33].

In spite of the extensive knowledge obtained so far, the thermal decomposition and combustion mechanisms of ADN are still not completely established. The purpose of the present work is to compile all the information on ADN thermal decomposition and combustion published to date and conduct a comprehensive survey of the research results. The basic thermal characteristics, chemical kinetics, and combustion behavior of ADN will be discussed systematically.

1. THERMAL DECOMPOSITION OF ADN

The study of ADN thermal decomposition consists primarily of visual observation of the phenomenon, identification of decomposition mechanisms and the ensuing products, kinetic analysis, and theoretical modeling. Similar studies on KDN and HDN are helpful in investigating the key physicochemical processes involved with ADN. Even though there are some inconsistencies in the observations reported in different works, a basic understanding of the mechanisms of ADN thermal decomposition has been achieved.

1.1. Overall Thermal Decomposition Characteristics

In comparison with KDN, sodium dinitramide (NaDN), and hexamethylenetetramine dinitramide (HMDN), ADN has the lowest decomposition temperature and the highest decomposition rate and heat release [39]. ADN is less stable thermally than KDN, but much more stable than NH_4NO_2 and alkyl dinitramide (alkyl-$N(NO_2)_2$) [2]. Among ammonium salts, the order of anion stability is $NO_3^- > N(NO_2)_2^- > NO_2^- >$ alkyl-$N(NO_2)_2$. The higher stability of $N(NO_2)_2^-$ is attributed to stabilization of the overall negative charge through the resonance effect [40]. The thermal stability of dinitramide metal salts depends on the metal cation electronegativity [11], and their higher electronegativity results in a higher decomposition rate. In dinitramide onium salts, such as hydrazinium, guanidinium, anilinium, and tetramethylammonium, basicity of the cation strongly influences the decomposition rate [41]. Bases with pKa < 5 have an order-of-magnitude greater decomposition rate as compared to based with pKa > 8. According to microcalorimetric analysis, the melted (prilled) ADN seems more thermally stable than pure (crystal) ADN [42], similar to KDN and NaDN. The decomposition rate of dinitramide metal salts in the solid phase is 10–10^3 times faster than in the liquid phase [11, 43, 44].

Water can inhibit the solid-phase decomposition in dinitramide metal salts. Such an inhibition leads to a lower rate of decomposition in the solid phase than in the liquid phase. Moist ADN containing 0.4–0.5% of water was more thermally stable than dry ADN containing 0.02–0.05% of water [45, 46]. Manelis' experiments [46] showed that the decomposition rate of relatively dry ADN with 0.05% of water was about 1000 times faster than that of moist ADN with 0.4% of water. The effect of water can be explained on the basis of the ionic reaction $HN(NO_2)_2 + H_2O \leftrightarrow H_3O^+ + N(NO_2)_2^-$. When a small amount of water was added to the ADN melt, the decomposition rate first decreased but later increased when the amount of water exceeded 5 mole % [27, 47].

ADN is less thermally stable and slightly more sensitive to mechanical impact than AP, HMX, and cyclotrimethylenetrinitramine (RDX) [6, 42, 45, 48]. Prilled ADN, however, showed much lower impact sensitivity than RDX [42]. ADN also has lower friction sensitivity than RDX. Hatano et al. [49] found that powdered and prismatic types of ADN were more sensitive thermally than the coagulated and needle types. ADN deflagrates due to hot-spot propagation under the impact action [48].

At a normal heating rate (15 K/min), direct visual observation [50] indicated that ADN begins to melt at about 92°C, and formation of small gaseous bubbles is observed at 120°C within the melt layer. These bubbles burst as they move toward the surface. At 150–160°C, nucleation (formation of larger gas bubbles) and bursting of gas bubbles increases considerably. Above 170°C, the liquid boils violently and evolves into large amounts of gases; a cloud of pale white is also observed. After melting, ADN immediately begins to decompose and form AN and N_2O at atmospheric pressure. Slow decomposition of ADN may begin in the solid phase at 60°C to produce gaseous N_2O [15, 37]. Under high-flux laser heating [24, 50] (e.g., 50 W/cm^2), non-luminous ignition of ADN occurs with evolution of a pale white (AN aerosol) or a brownish tinted particle cloud (NO_2).

The overall characteristics of ADN thermal decomposition can be obtained from the DSC spectra reported in [35, 36, 28, 39, 42, 2, 26]. As is listed in Table 1, depending on ADN samples and experimental conditions, the onset of thermal decomposition is at $T_{\text{decomp}} = 150$–155°C and the exothermic peak is observed around $T_{\text{exo}} \approx 180$–198°C. The decomposition temperature range of 150–155°C based on DSC coincides with that obtained from MS, FTIR, and TGA [15, 25, 36, 37, 50].

Tompa [28] conducted DSC and TGA investigations for several kinds of ADN samples (prilled, unprilled, and recrystallized) under various experimental conditions (in aluminum and gold-coated aluminum pans; in sealed glass ampoules; under vacuum and pressure). Results obtained from the DSC spectra showed asymmetrical or double exothermic peaks with an endothermic peak at a higher temperature. Tompa [28] performed another test in which the ADN sample first underwent an isothermal (52/62°C) TGA process to obtain a residue, followed by the DSC. The residue analysis revealed an endothermic peak at 59°C and a lower melting point (83°C) attributed to the presence of AN. It was noted that the first exothermic peak [28] was near the melting point (169.6°C) of AN, and the additional exothermic peak was at 310°C, close to the AN decomposition temperature (280–320°C). In the TGA experiments at a low heating rate of 0.5 K/min, Lobbecke et al. [26] observed the onset of thermal decomposition at 126.8°C followed by a symmetrical exothermic peak. The exothermic decomposition of ADN proceeded in two steps [26]. The first step resulted in a ≈30% mass loss at $T = 160$°C, and the second step consumed the remaining ≈70% of mass at $T = 160$–230°C. The evolution of N_2O in the reaction $ADN \rightarrow N_2O + AN$ resulted in a mass loss of 35%. Therefore, the two steps are possibly correlated to ADN decomposition into AN and subsequent AN decomposition.

The pressure–temperature reaction phase diagram of ADN [14] showed that, in the high pressure (2.0–10.0 GPa) and temperature (120–140°C) ranges, β-ADN underwent a solid-state molecular rearrangement to form AN and N_2O. This is accompanied by a decrease in volume. The FTIR analysis of the experimental sample at

TABLE 1

DSC Thermal Analysis of ADN with Different Heating Rates dT/dt

dT/dt, K/min	T_{decomp}, °C	T_{exo}, °C	Reference
5	150	180	[36]
5	150	180.3	[39]
10	154.4	198	[2]
10	150	190	[42]
15	160	190	[50], DTA
20	150	189	[35]
0.5	126.8	159.3	Modulated DSC method [26]

Note. The modulated DSC method refers to an experiment that was carried out at a linear heating rate of 0.5 K/min superimposed by a sinusoidal temperature variation, in order to improve resolution and enhance sensitivity of the DSC.

2.5 GPa offered direct evidence for such a molecular rearrangement in the solid phase. For high pressures, the FTIR spectrum of β-ADN did not reveal any significant change at 125°C as compared to that at room temperature; at 145°C, however, strong absorption of N_2O at $\lambda = 2\,223\ \text{cm}^{-1}$ appeared. This absorption band existed even when the temperature was decreased to 50°C at 2.5 GPa, implying an irreversible change. When the pressure was decreased to 1 atm, the absorption signal at $\lambda = 2223\ \text{cm}^{-1}$ disappeared because of the emergence of the N_2O gas from the solid phase. The residue was identified to be AN. Thus, the crystalline structure of ADN tends to release N_2O during its decomposition.

Thermal decomposition of ADN and other dinitramide salts exhibit characteristics of base stability and acid catalysis [2, 15, 47]. HNO_3 is one of the decomposition products of ADN, and the addition of HNO_3 aqueous solution to the ADN melt accelerates decomposition [47]. In strong acids, such as H_2SO_4 and HNO_3, ADN decomposes more rapidly at room temperature as the rate of acid-catalytic decomposition is proportional to acidity. The NO_2 gas was found to catalyze ADN decomposition [35, 36], whereas the basic substances, such as NH_3, NH_4F, amine, and urea, may restrain ADN decomposition. Hexamethylenamine, 2-nitrodiphenylamine, methyldiphenylurea cyanoquanidine, and prophosphatrane compounds improve the thermal stability of ADN [51]. Spheres of prilled ADN + 0.3% of hexamine exhibited excellent thermal stability [45], but addition of 2% of hexamine increased their friction sensitivity. Free radical scavengers, such as 2,6-di-*tert*-butyl phenol, did not increase the thermal stability of ADN [15].

ADN in an aqueous solution is light sensitive [16, 42]. Ultraviolet light photolysis of ADN and AN was studied by means of electron spin resonance (ESR) spin trapping of the $NO_2\cdot$ radical [16]. The nitromethane anion $CH_2{=}NO_2^-$ was used to trap the $NO_2\cdot$ radical, producing the dinitromethyl anion (DNM·). Formation of $NO_2\cdot$ in ADN followed a first-order rate law of photolysis, while the kinetic data of $NO_2\cdot$ growth in AN were consistent with a zero-order rate law. This implies that the rate of formation of $NO_2\cdot$ in ADN under photolysis conditions is faster than that in AN.

1.2. Thermal Decomposition Products

NH_3, $HN(NO_2)_2$, $HNNO_2$, HNO_3, N_2O, NO_2, NO, H_2O, N_2, and AN are anticipated to be the prominent decomposition products of ADN pyrolysis, and their evolution rates depend on temperature and pressure. The temporal or temperature sequences of decomposition products are different in different papers, as is seen from Table 2. Approximate stoichiometric equations for ADN thermal decomposition under various experimental conditions are summarized in Table 3.

N_2O evolution is one of the main characteristics of ADN thermal decomposition. Early detection of N_2O was reported by many researchers [15, 21, 37]. It was even detected at $T = 60°\text{C}$ in the solid phase [15]. In most cases, N_2O appeared before NO_2 and became more abundant than NO_2 with increasing temperature. According to Oxley et al. [35], high concentrations of N_2O, N_2, and AN were observed under isothermal and sealed conditions, but NO_2 and NH_3 were almost totally absent. NO_2 was detected above 150°C through an MS analysis by Rossi et al. [25] and by an FTIR analysis by Russell et al. [15]. NO and N_2O were detected earlier than NO_2 and in larger amounts [25]. In the MS-pyrolysis experiments [29], NO_2 in the gas phase was not reported, due to the assignment of the NO_2 peak ($m/z = 46$) to the HDN molecule. Vyazovkin and Wight [37] observed an earlier appearance of NO_2 [N_2O_4 dimer] and NO [$(NO)_2$ dimer] than N_2O using TGA–MS and FTIR-pyrolysis, while with laser pyrolysis, N_2O and NO_2 were detected simultaneously.

The decomposition mechanism ADN → NH_3 + HDN suggests that NH_3 evolution should occur early, but the experimental measurements have shown inconsistent results. When ADN was heated to 260°C at a rate of 2000°C/sec on a platinum filament [21], FTIR detected NH_3, N_2O, and HNO_3 in similar amounts in the initial spectra; then, the amounts of N_2O and NO_2 increased, and the amounts of NH_3 and HNO_3 decreased sharply. In the laser-pyrolysis experiments [24] with flux densities of 20–30 W/cm^2, the microprobe MS indicated only 1–1.5% or barely detectable NH_3. Vyazovkin and Wight [37], in the range $T = 25$–$250°\text{C}$ at a heating rate of 5°C/min, found that NH_3 appeared only above 100°C, much later than NO_2 and N_2O. NH_3 was not detected until 180°C in the TGA/FTIR analysis at a heating rate of 5°C/min [15]. NH_3 and HDN were possibly being absorbed in the condensed phase at low temperatures. However, MS-pyrolysis under vacuum [25, 29, 33] provided adequate evidence of a substantial quantity of NH_3.

N_2 and H_2O are not the most typical initial decomposition products. At low temperatures or in vacuum, ADN decomposition produces only small amounts of N_2 and H_2O. Under fast pyrolysis [21, 24], N_2 and H_2O were formed in relatively larger amounts. Isothermal decomposition of ADN in a sealed glass tube [35] showed a tendency to produce more N_2. For decomposition of neat ADN at $T = 230°\text{C}$, the amount of N_2 was nearly the same as that of N_2O (mole ratio

TABLE 2

Gaseous Products of ADN Decomposition under Different Heating Conditions

Experimental conditions	Products detected	Reference
Heating rate 20°C/sec	N_2O for 60°C AN_{subl} for 80°C N_2O, ADN_{subl}, and AN_{subl} for 95°C NO_2, N_2O, ADN_{subl}, and AN_{subl} for 150°C NH_3, NO_2, and AN_{subl} for 180°C	[15]
Isothermal heating	N_2O and AN_{subl} for 60–90°C N_2O, AN_{subl}, and ADN_{subl} for 95–120°C, NO_2, N_2O, ADN_{subl}, and AN_{subl} for 130–160°C	
Pyrolysis under vacuum	NH_3 and N_2O (dominant) for 90°C NH_3, N_2O (dominant), H_2O, and NO for 130°C HN_3, N_2O (dominant), H_2O, NO, and HDN for 150°C $NH_3 \sim N_2O \sim H_2O \sim NO$ (comparable amounts) and HDN (in its maximum) for 170°C	[25]
Pyrolysis in the gas cell at 5°C/min	N_2O_4 and HNO_3 for 50°C N_2O for >50°C NO, and H_3 for >100°C	[37]
Fast pyrolysis (2000°C/sec)	$NH_3 \sim N_2O \sim HNO_3$ (in nearly identical amounts) at the beginning $N_2O\uparrow$, $NO_2\uparrow$, $AN\uparrow$, $NH_3\downarrow$, and $HNO_3\downarrow$ in the middle $N_2O\uparrow$; $NH_3\downarrow$; $HNO_3\downarrow$; NO_2, NO, AN (constant) at the end	[21]
Laser pyrolysis (flux density 20–30 W/cm^2)	N_2O and H_2O; then, NO_2, then NO and N_2, and at the end, NH_3	[24]

Note. The subscript "subl" refers to sublimation.

TABLE 3

Stoichiometry of ADN Thermal Decomposition

Stoichiometric equations	Experimental conditions	Reference
$ADN \to 0.07NH_3 + 0.33H_2O + 0.22N_2O + 0.13NO_2 + 0.13N_2 + 0.05NO + 0.02HNO_3 + 0.05AN$	260°C; Pt filament; 1 atm; heating rate 2000°C/sec	[21]
$ADN \to 0.03NH_3 + 0.31H_2O + 0.29N_2O + 0.08NO_2 + 0.13N_2 + 0.01NO + 0.15AN$	Laser pyrolysis (100 W/cm^2; 1 atm)	[24]
$ADN \to 0.65N_2O + 0.44N_2 + 0.46AN + 0.22ADN$ (78% decomposition extent)	Isothermal conditions; 200°C, sealed glass tube	[35]
$ADN \to 0.76N_2O + 0.35N_2 + 0.376H_2O + 0.14HNO_3 + 0.81AN$ (8.5% decomposition extent)	Isothermal conditions; 106.2°C, sealed glass ampoule	[41]

$N_2/N_2O = 0.6$–0.8); for ADN in an aqueous solution at $T = 200$°C, the amounts of N_2 and N_2O were 0.15 and 0.69 mole per ADN mole, respectively. The ^{15}N isotope analysis showed that 90% of N_2 came from a combination of one N atom in ammonium and one N atom in the nitro-group, and 90% of N_2O consisted of one N atom in the amine and one N atom in the nitro-group. Laser pyrolysis at 20 W/cm^2 by Fetherolf and Litzinger [24] indicated that the mole fraction of H_2O was about half that of N_2O and was approximately equal to that of N_2O at 30 W/cm^2.

The presence of HDN is important in establishing ADN thermal decomposition mechanisms. HDN was detected in some pyrolysis experiments in vacuum [25, 29, 33]. In the test conducted by Rossi et al. [25] at high vacuum (10^{-8} torr), FTIR detected HDN and recombination of ADN from NH_3 and HDN, while MS detected free HDN [$m/z = 46$ (NO_2^+) and 60 (NNO_2^+)]. A MS-pyrolysis analysis by Korobeinichev et al. [29] (10^{-6}, 6, and 100 torr and 1 atm) assigned $m/z = 46$ (NO_2^+) to HDN through a comparison of relative intensities of mass peaks. Nevertheless, the mass peak $m/z = 60$ for NNO_2^+ was not detected. The FTIR-pyrolysis by Brill et al. [21] did not detect HDN. It was assumed [21, 37] that HDN homolyzes in the condensed phase.

FTIR seems to be more effective in detecting HNO_3. Vyazovkin and Wight [37] found that, at $T = 50°C$, HNO_3 evolved almost simultaneously with NO_2, and its concentration increased. Brill et al. [21] observed almost equal amounts of HNO_3, NH_3, and N_2O in the initial spectra of fast ADN pyrolysis and a sharp decrease in concentrations after that. The MS-pyrolysis investigations by Fetherolf and Litzinger [24] and Rossi et al. [25] did not detect HNO_3, possibly due to heterogeneous decomposition of HNO_3 on metal walls or within the probe.

AN is one of the main products of ADN thermal decomposition. Lobbecke et al. [26] detected an infrared absorption band of sublimated AN at 3176–3281 cm^{-1}, and Russell et al. [15] observed AN sublimation even at 80°C. The pale white AN aerosol was visually observed by many researchers [21, 24, 50] during ADN pyrolysis. At high pressures ($p > 2.5$ GPa), ADN can be transformed into AN through a solid-phase molecular rearrangement [14].

As the preceding summary suggests, different gas products and concentrations have been observed in ADN decomposition, depending on experimental techniques and conditions, so that a number of different suggestions have been made as to the thermal decomposition mechanisms.

1.3. Thermal Decomposition Kinetics

The ADN thermal decomposition kinetics depends on several factors, such as temperature, pressure, isothermal or non-isothermal conditions, extent of the reaction, catalysis, and species observed. The activation energies (E_a) reported by various researchers range within 21–43 kcal/mole, depending on samples and experimental methods, and the values fall between 35 and 43 kcal/mole in most cases. The DSC data from the ASTM[3] give $E_a = 27$ kcal/mole. For HDN, the theoretically calculated energy required for $N—NO_2$ bond cleavage is 38–40 kcal/mole, and E_a for thermal decomposition of AN is also about 40 kcal/mole [52]. Some activation-energy data with the corresponding experimental techniques and conditions are summarized in Table 4.

According to Oxley et al. [35], in temperature ranges of 120–160°C and 160–240°C, ADN thermal decomposition in a sealed glass tube showed activation energies $E_a = 18$ and 35–40 kcal/mole, respectively. Since the onset of rapid decomposition of ADN occurs at 155–160°C, the existence of different decomposition mechanisms above and below 160°C seems reasonable. Vyazovkin and Wight [36, 38] used a nonlinear isoconversional method to treat TGA data for ADN to overcome the dependence of E_a on the reaction model and to establish a relationship between E_a and the extent of the reaction. The activation energy E_a was found to be (41.8±5) kcal/mole at the initial stage and (30±5) kcal/mole at the end of decomposition, showing a marked decrease with the extent of the reaction. The higher E_a at the initial stage is attributed to N_2O elimination from the dinitramide anion in ADN, and the variation of E_a with the reaction extent correlates with the transition of ADN to AN. ADN behaved differently during isothermal and non-isothermal decomposition at $T = 132$–$150°C$ [36, 38]. In the isothermal case, the activation energy did not show a strong dependence on the reaction extent and reached 32.3–33.5 kcal/mole for the reaction extent between 0.2 and 0.8. Non-isothermal decomposition at $T = 125$–$220°C$ required a higher activation energy than isothermal decomposition at 132–150°C.

Santhosh et al. [53] obtained $E_a = 39.2$ kcal/mole with a frequency factor of $1.52 \cdot 10^4$ min^{-1} by DSC. Their TGA data revealed the change in E_a from 41.6 to 16.4 kcal/mole with the conversion extent varied from 10 to 90%. Hommel and Trubert [54] obtained $E_a = 56.7$ kcal/mole with a frequency factor of $1.2 \cdot 10^{26}$ sec^{-1} using DSC. Korobeinichev et al. [29] suggested the initial decomposition reaction $ADN(g) + M \rightarrow NH_3 + HN(NO_2)_2 + M$ with a preexponent $A = 3.2 \cdot 10^{12}$ $cm^3 \cdot mole^{-1} \cdot sec^{-1}$ and $E_a = 11.5$ kcal/mole. The latter is in agreement with the theoretical value $E_a = 12$–14 kcal/mole for ADN(g) dissociation into NH_3 and $HN(NO_2)_2$ [23].

Oxley et al. [35] observed that NO_2 catalyzes ADN decomposition. A less pronounced decrease in E_a with increasing reaction extent at a high flow rate of the carrier gas was believed to be evidence for the catalytic action of NO_2 [36]. A DSC investigation by Tompa et al. [39] showed that ADN decomposition in a sealed pan had a lower E_a than that in an unsealed pan with a pin-hole. A lower value ($E_a = 29.5$ kcal/mole) was observed under pressurized conditions (air or He) than at one atmosphere (N_2 or He). The DSC results also suggest that ADN decomposition has a low activation energy in vacuum.

There exists some theoretical and experimental evidence for acid-catalyzed decomposition [21, 27, 55] of ADN. Thermal decomposition of the ADN melt was found to be self-accelerated at the initial stage owing to HNO_3 accumulation. The increase in the decomposition rate is attributed to the equilibrium reaction $HNO_3 + N(NO_2)_2^- \rightleftarrows NO_3^- + HN(NO_2)_2$. The decomposition rate of $HN(NO_2)_2$ is 10^7–10^8 times higher than

---

[3] American Society for Testing of Materials

TABLE 4

Activation Energies of ADN Thermal Decomposition

Experimental conditions	E_a, kcal/mole	Reference
DSC (N_2)	41.9	[28]
DSC (He)	43.1	
DSC (sealed pan)	30.8	
DSC ($p = 37.42$ atm, air)	29.3	
DSC ($p = 37.42$ atm, He)	29.5	
DSC (vacuum, 35 mm Hg)	31.2	
Isothermal experiments in a sealed glass tube	37.8; ADN: $[NH_4^+]$	[35]
	39.9; $[N(NO_2)_2^-]$	
	35.3; gas products	
	36.3; 1% H_2O; ADN $[N(NO_2)_2^-]$	
	37.6; 20% H_2O; ADN $[N(NO_2)_2^-]$	
TGA (u is the carrier-gas flow rate, ml/min; a is the extent of the reaction)	42 $u/a = 30/0.1$	[36]
	40 100/0.1	
	31 30/0.5	
	36 100/0.5	
DSC (thermal ignition in Wood's metal bath for 165–200°C)	37.8	[42]
	30.4	

that of $N(NO_2)_2^-$ for $T = 0$–$100°C$ [27, 47, 56, 57] since the anion $N(NO_2)_2^-$ has a higher activation energy than $HN(NO_2)_2$. Further, the protonated $H_2N(NO_2)_2^+$ has a more rapid decomposition rate than $HN(NO_2)_2$. $N(NO_2)_2^-$ appeared to be extremely unreactive for a wide variety of reagents [58] due to the high stability resulting from its resonance-delocalized structures. For $N(NO_2)_2^-$ in a solution, $E_a = 41$ kcal/mole [27], and the energy calculated by Politzer et al. [59] for the reaction $N(NO_2)_2^- \rightarrow NNO_2^- + NO_2 \rightarrow N_2O + NO_3^-$ was 49.8 kcal/mole. For the reaction $HN(NO_2)_2 \rightarrow NO_2 + HNNO_2$, $E_a = 35$ kcal/mole [33]. The poor stability of $HN(NO_2)_2$ may be attributed to a weaker N—N bond in $HN(NO_2)_2$ as compared with $N(NO_2)_2^-$. The N—N in $N(NO_2)_2^-$ has a bond order between the double (N=N) and single (N—N) bonds, while N—N in $N(NO_2)_2$ and in protonated $H_2N(NO_2)_2^+$ has a bond order closer to a single N—N bond. The nitro-form $HN(NO_2)_2$ is of lower N—N bond order than the acido-form $HON(O)NNO_2$ and protonated $H_2N(NO_2)_2^+$ [57] [the acido-form $HON(O)NNO_2$ and the nitro-form $HN(NO_2)_2$ are tautomeric]. Kazakov et al. [57] claimed that HDN decomposes through the nitro-form $HN(NO_2)_2$ into $N_2O + HNO_3$. Bottaro et al. [2] studied the kinetics of ADN decomposition in a concentrated acid, where UV absorbency at 212 nm and 284 nm were used to measure the rate constant and the half-decay time in sulfuric acid at room temperature. No loss of ADN was observed with a sulfuric acid concentration of 8.0 mole/liter in 8 h. When the acid concentration was 11.0 mole/liter or higher, however, the ADN loss was detected in minutes.

1.4. Initial Thermal-Decomposition Reactions

Many theoretical [22, 23, 47, 55, 59] and experimental [21, 24–29, 33–38] investigations have been performed to study the mechanisms of thermal decomposition of ADN. Mebel et al. [23] considered the structures and decomposition products of ADN in the gas phase theoretically and described the potential energy surface of early decomposition reactions. After vaporization of ADN(s) with a sublimation heat H_{subl}, ADN(g) molecules exist only in two kinds of complex structures: $[NH_3] \cdot [HN(NO_2)_2]$ and $[NH_3] \cdot [HON(O)NNO_2]$. The latter structure is less stable; the difference in activation energies is $\Delta E = 2.3$ kcal/mole. The calculated heats of formation ΔH_f^0 (0 K) for gaseous $[NH_3] \cdot [HN(NO_2)_2]$ and $HN(NO_2)_2$ are 2.3 and 24.9 kcal/mole, respectively. For $HN(NO_2)_2$, Michels and Montgomery [40] and Politzer et al. [22] reported

ΔH_f^0 (0 K) = 28.4–29.7 kcal/mole and ΔHf^0 (298 K) = 19 kcal/mole, respectively. ADN(g) dissociates into $NH_3 + HN(NO_2)_2$ [or $HON(O)NNO_2$] with E_a = 12–14 kcal/mole [23]. The energy barrier for NO_2 elimination from $HN(NO_2)_2$ and $HON(O)NNO_2$ (i.e., N—NO_2 bond energy) is 38–40 kcal/mole.

Lin and Park [33] conducted kinetic modeling with *ab initio* MO/RRKM calculations. With the use of a detailed mechanism involving the initial decomposition step $ADN(g) \rightarrow NH_3 + HN(NO_2)_2$ and 152 reactions, good agreement was achieved between the calculated species concentration profiles and experimental results of ADN sublimation–pyrolysis mass spectrometry at high vacuum [(5–10) $\cdot 10^{-5}$ torr]. When 9% of $HN(NO_2)_2$ were replaced by HNO_3 and N_2O, the agreement was slightly improved. The reaction $ADN(g) \rightarrow NH_3 + HN(NO_2)_2$ was supported by an experimental study of decomposition kinetics under vacuum [33].

The reaction $HDN \rightarrow N_2O + HNO_3$ could not proceed by a simple bond cleavage. It needs to undergo a four-member molecular rearrangement ($O_2\{NONN\}O$) or proceed through other transition states [2, 14, 22, 35, 59, 60]. The solid-phase rearrangement of ADN with formation of AN and N_2O was observed by Russell et al. [14], and the gas-phase rearrangement of $N(NO_2)_2^- \rightarrow N_2O + NO_3^-$ was observed by Doyle [60]. Politzer et al. [59] did not find the four-member molecular rearrangement but pointed out that the transition reaction $N(NO_2)_2^- \rightarrow NNO_2^- + NO_2 \rightarrow N_2O + NO_3^-$ has the lowest E_a requirement and, hence, is the most probable one. It was suggested that NNO_2^- and NO_2 have the option of forming a very loosely-bound complex through electrostatic interactions between the negative oxygen in NNO_2^- and the positive nitrogen in NO_2. The complex can subsequently dissociate to form N_2O and NO_3^-.

The theoretical research by Michels and Montgomery [40] and Politzer et al. [59] largely supported the case for dissociation of $HON(O)NNO_2$ into N_2O and HNO_3, while the results of Mebel et al. [23] tend to support the N—NO_2 bond cleavage of $HN(NO_2)_2$ forming NO_2 with no acid catalysis. The activation energy for the reaction $HON(O)NNO_2 \rightarrow N_2O + HNO_3$ (42.2 kcal/mole) was higher than that for N—NO_2 cleavage [23] (38–40 kcal/mole). Nevertheless, the reaction may be acid-catalyzed in the presence of H^+ [2, 22, 55]. Michels and Montgomery [40] reported a high value of E_a (48 ± 8 kcal/mole) for $HN(NO_2) \rightarrow NO_2 + HNNO_2$ and pointed out that the unimolecular decomposition mechanism (four-member mechanism $O_2\{NONN\}O^- \rightarrow N_2O + NO_3^-$) has a lower activation energy (27 kcal/mole) than that of N—NO_2 bond cleavage. The proposed initial thermal decomposition reactions of ADN are listed in Table 5.

1.5. Initial Decomposition Mechanisms

Important reactions in the ADN thermal-decomposition mechanisms are

$$ADN \rightarrow NH_3 + HDN, \tag{R1}$$

$$ADN \rightarrow NH_3 + N_2O + HNO_3, \tag{R2}$$

$$ADN \rightarrow N_2O + AN, \tag{R3}$$

$$HDN \rightarrow N_2O + HNO_3, \tag{R4}$$

$$HDN \rightarrow N_2O + HNNO_2, \tag{R5}$$

$$NH_3 + HNO_3 \rightarrow AN\ (\text{aerosol}), \tag{R6}$$

$$\begin{aligned} ADN(s) &\rightarrow [NH_3] \cdot [HN(NO_2)_2](g) \\ &\rightarrow NH_3 + HN(NO_2)_2, \end{aligned} \tag{R7}$$

$$\begin{aligned} ADN(s) &\rightarrow [NH_3] \cdot [HON(O)NNO_2](g) \\ &\rightarrow NH_3 + HON(O)NNO_2. \end{aligned} \tag{R8}$$

Hereafter, the solid, liquid, and gas phases are denoted by (s), (liq), and (g), respectively. Experimental validation of (R1) and (R2) was based on the early detection of NH_3 along with N_2O, NO_2 and HNO_3, while that of (R3) is based on the appearance of N_2O, NO_2, and NO with no early trace of NH_3. Considering the poor stability of HDN and the recombination reaction (R6) involving NH_3 and HNO_3, (R2) may be considered as a combination of (R1) and (R4), and (R3) may be a result of (R1)→(R4)→(R6). The evidence suggesting that reaction (R1), (R7), or (R8) forms NH_3 and HDN are listed below:

1. Rossi et al. [25] detected HDN and regenerated ADN by FTIR under high vacuum (10^{-8} torr).
2. Korobeinichev et al. [29] studied ADN deposition at the exit of a flow reactor (vacuum, 6 torr). By analyzing the peak intensities in mass spectra of ADN thermal decomposition at $p = 10^{-5}$, 6, and 100 torr and 1 atm, they assigned the peak $m/z = 46$ (NO_2) to the HDN molecule.
3. Lin and Park [33] conducted experiments on thermal decomposition of sublimed ADN and developed a detailed kinetic model consisting of a total of 152 reactions to validate the prevalence of (R1).
4. Collision-induced dissociation spectra of $[NH_4N(NO_2)_2]_nNH_4^+$ aggregate ions considered by Doyle [60] showed that a single $HN(NO_2)_2$ molecule can dissociate from the parent aggregate ions.
5. Acid catalysis and base stability of ADN decomposition support the production of HDN.

TABLE 5

Initial Stoichiometric Pathways of ADN Thermal Decomposition

Main reactants	Reactions	ΔH (298 K), kcal/mole [22]
ADN	$NH_4N(NO_2)_2 \rightarrow NH_3 + HN(NO_2)_2$	44
	$NH_4N(NO_2)_2 \rightarrow NH_3 + N_2O + HNO_3$	11.5^a
	$NH_4N(NO_2)_2 \rightarrow N_2O + NH_4NO_3$	−32
	$NH_4N(NO_2)_2(s) \rightarrow [NH_3] \cdot [HN(NO_2)_2](g) \rightarrow NH_3 + HN(NO_2)_2)$	
	$NH_4N(NO_2)_2(s) \rightarrow [NH_3] \cdot [HON(O)NNO_2](g) \rightarrow NH_3 + HO N(O)NNO_2$	
	$NH_4N(NO_2)_2 \rightarrow NO_2 + NH_4NNO_2$	
	$NH_4N(NO_2)_2 \rightarrow NO_2 + NO + NH_4NO$	
	$NH_4N(NO_2)_2(s) \rightarrow NH_4^+ + N(NO_2)_2^- \rightarrow NH_3 + HN(NO_2)_2$	144^b
HDN	$HN(NO_2)_2 \rightarrow N_2O + HNO_3$	
	$HN(NO_2)_2 \rightarrow NO_2 + HNNO_2$	
	$HON(O)NNO_2 \rightarrow N_2O + HNO_3$	33.8
	$HON(O)NNO_2 \rightarrow NO_2 + HON(O)N$	36.3
	$N(NO_2)_2^- \rightarrow N_2O + NO_3^-$	−17.1
	$N(NO_2)_2^- \rightarrow NO_2 + NNO_2^-$	49.7
	$2HN(NO_2)_2 \rightarrow 2N_2O + 2NO + 1.5O_2 + H_2O$	
	$2HN(NO_2)_2 \rightarrow 3NO_2 + NO + N_2 + H_2O$	
AN	$NH_3 + HNO_3 \rightarrow NH_4NO_3$ (aerosol)	—
	$NH_4NO_3(liq) \rightarrow NH_3 + HNO_3$	44; 38.92 (200°C)^c
	$5NH_4NO_3(liq) \rightarrow 4N_2 + 2HNO_3 + 9H_2O$	-35^a
	$NH_4NO_3(liq) \rightarrow N_2O + H_2O$	−13.5 (200°C)^d
	$NH_4NO_3(s) \rightarrow NH_4^+ + NO_3^- \rightarrow NH_3 + HNO_3$	162^e
NH_3	$2NH_3 + 2NO_2 \rightarrow NH_4NO_3$ (aerosol) $+ N_2 + H_2O$	
	$2NH_3 + 2NO_2 \rightarrow N_2O + N_2 + 3H_2O$	
	$4NH_3 + 4NO_2 \rightarrow 2NO + 3N_2 + 6H_2O$	-309^a
	$NH_3 + NO_2 \rightarrow NH_2 + HONO$	29
HNO_3	$2HNO_3 \rightarrow 2NO_2 + H_2O + 1/2O_2$	—
	$2HNO_3 \rightarrow 2NO + H_2O + 1.5O_2$	

Note. The data marked by the superscripts a, c, and d refer to papers [21], [61], and [62], respectively; the data marked by the superscripts b and e refer to ADN and AN lattice enthalpy, respectively.

6. Brill et al. [21], Russell et al. [15], and Fetherolf and Litzinger [24] suggested the reaction mechanism (R1) under conditions of rapid pyrolysis or high temperatures.

7. Lobbecke et al. [26] proposed that (R1) is the first step of ADN decomposition.

8. Theoretical calculations by Mebel et al. [23].

Reaction (R1) predicts early formation of a large amount of NH_3. Some experiments where NH_3 appeared quite late or was barely detected did not favor (R1). Brill et al. [21] and Vyazovkin and Wight [37] could not find HDN by an *in-situ* FTIR analysis. Brill et al. [21] postulated that HDN may homolyze into $HNNO_2$ and NO_2 in the condensed phase, but $HNNO_2$

was not found in the FTIR spectra either. According to Fetherolf and Litzinger [24], NH_3 was barely detectable in laser-induced pyrolysis of ADN pellets. In the DSC and TGA analyses of ADN, Russell et al. [15] did not observe the appearance of NH_3 below 188°C.

The theory that ADN undergoes a molecular rearrangement is supported by many theoretical and experimental studies. The four-center rearrangement $O_2\{NONN\}O^-$ contributes to the conversion of the ADN crystal to AN and N_2O at very high pressures [14], while Doyle [60] mentioned that the gas-phase rearrangement of $N(NO_2)_2^-$ could occur to produce N_2O and NO_3^-. According to Gilardi et al. [6–9], there are strong hydrogen-bonding networks in the ADN crystal, involving all four hydrogen atoms. This makes the elimination of NH_3 from the solid ADN more difficult. Doyle's study [60] revealed a large number of aggregate $[NH_4N(NO_2)_2]_nN(NO_2)_2^-$ and $[NH_4N(NO_2)_2]_nNH_4^+$ (n = 2–21) ions in the gas phase. According to the theoretical studies by Alavi and Thompson [63], the hydrogen bonding stabilizes a single ADN molecule; however, in an ADN cluster, the $N{-}H\cdots O$ hydrogen bonds cause the proton transfer and change the structure of the dinitramide group. These structural rearrangements facilitate reaction (R3). Before melting, the crystal ADN has a lesser tendency to form NH_3 and HDN and is more likely to produce N_2O. Thus, it can be speculated that reaction (R3) is responsible for decomposition in the solid phase of ADN, and high-pressure conditions facilitate this decomposition. The evidence supporting the case for (R3), which follows a low E_a pathway, is listed below.

1. The irregular exothermic peak or double exothermic peaks in the DSC curves of thermal decomposition of ADN imply the involvement of AN thermal properties, since the peak temperature around 180–200°C is close to the melting point (170°C) of AN and there is an additional endothermic peak attributed to AN sublimation.

2. Vyazovkin and Wight [36, 38] found that E_a decreased from 41.8 to 30 kcal/mole as the extent of the reaction increased. The phenomenon was considered to be evidence of formation of a large amount of AN.

3. According to Russell et al. [14, 15], the solid-state molecular rearrangement of ADN may occur to form AN and N_2O under very high pressures. They observed the early evolution of considerable amounts of N_2O and AN, followed by NO_2. NH_3 appeared only when the temperature rose to 188°C.

4. Vyazovkin and Wight [37] found the evolution of NO_2, N_2O, and NO, and did not find NH_3 below 100°C.

5. Fetherolf and Litzinger [24] observed early evolution of abundant N_2O and H_2O, but with only 1–1.5% or barely detectable NH_3 (at pressures of 0.1 and 0.3 atm).

6. Oxley et al. [35] detected large amounts of N_2O and N_2 in isothermal decomposition of ADN in a sealed glass tube, without the appearance of NO_2.

7. Lobbecke et al. [26] observed a 30% mass loss at the initial stage of ADN decomposition, a phenomenon attributed to the evolution of the N_2O gas and production of AN.

8. Cliff et al.'s research [64] on thermal decomposition of alkali metal (Li, Na, K, Rb, and Cs) dinitramide showed that these salts thermally decompose into metal nitrates.

Factors disadvantageous to reaction (R1) seem to be advantageous to reaction (R3).

The following reactions could possibly occur in the solid-phase ADN decomposition:

$$\mathrm{ADN} \rightarrow NO_2 + NH_4NNO_2, \tag{R9}$$

$$\mathrm{ADN} \rightarrow NO_2 + NO + NH_4NO. \tag{R10}$$

No theoretical description of reaction (R2) is presently available. The experimental evidence provided by Brill et al. [21] showed comparable amounts of NH_3, N_2O, and HNO_3 at the initial stage of rapid ADN pyrolysis at a fixed temperature of 260°C. They proposed that products of ADN pyrolysis under rapid heating conditions should be NH_3 and $HN(NO_2)_2$. The $HN(NO_2)_2$ molecule could not be detected as it probably homolyzes to NO_2 and $HNNO_2$ in the condensed phase at high temperatures. HDN began to decompose at 70°C and was consumed completely at 140°C [25]. Given a low E_a, it is easy to obtain N_2O and HNO_3 from HDN through an intramolecular rearrangement. In most cases, nevertheless, it is difficult to differentiate clearly between reactions (R2) and (R1)→(R4) if (R4) occurs rapidly.

Many researchers detected the evolution of NH_3 above 100°C (i.e., above the ADN melting point, 92–95°C). Formation of NH_3 may result from either reaction (R1) or reaction (R2). When ADN melts, hydrogen-bonding interactions among the molecules become weak, and elimination of NH_3 becomes relatively easier than that in the solid phase. The fact that no HDN is detected in the range $T = 100$–155°C also seems to support the production of NH_3 from (R2). Further, if (R1) prominently occurs only under vacuum or after ADN sublimation and vaporization, then (R2) is more probable in condensed-phase decomposition of melted ADN at atmospheric or higher pressure. Thus, it is suggested that the unimolecular decomposition reaction (R2) contributes substantially to evolution of NH_3 and HNO_3 in the condensed phase, but (R3) competes with (R2). Owing to vaporization of a certain amount of melted ADN, reaction (R2) also occurs in the gas phase, though in competition with (R1). HDN produced by (R1) decomposes into N_2O and HNO_3 or NO_2 and into $HNNO_2$. Above 155°C, as a consequence of vaporization of a substantial amount of ADN, the condensed phase becomes a foam layer. In the gas phase, unimolecular dissociation of ADN(g) prevails through the pathways (R1)→(R4), (R1)→(R5), and (R2). The main exothermic reaction involves oxidation of NH_3 by NO_2, where HNO_3 contributes to NO_2 formation through the reaction $HNO_3 \rightarrow NO_2 + H_2O + O_2$.

From the kinetics viewpoint, thermal decomposition of ADN exhibits two stages with low and high activation energies, below and above 160°C, respectively. The low activation energy (<30 kcal/mole) can possibly be attributed to condensed-phase dissociation of ADN, and the high activation energy (about 40 kcal/mole) to gas-phase dissociation of ADN. The molecular rearrangements ADN $\rightarrow$ N_2O + AN and ADN $\rightarrow NH_3 + N_2O + HNO_3$ are responsible for the first stage with a low activation energy and temperatures below 155°C. The mechanisms ADN $\rightarrow NH_3$ + HDN and HDN $\rightarrow NO_2 + HNNO_2$ are related to the second stage with a high activation energy. For ADN decomposition in an aqueous solution, however, Oxley et al. [35] obtained a linear Arrhenius plot in the temperature range of 120–240°C, which does not show the presence of two activation energies above and below 160°C. Neat ADN and ADN in an aqueous solution had similar decomposition rates [35].

The results of theoretical and experimental research on initial thermal decomposition of ADN can be consolidated on the basis of the discussion presented above. Its temperature-pressure dependences are summarized in Table 6. Reaction (R1) is dominant under vacuum and low pressures. At elevated pressures, (R3) is favored. During ADN combustion, especially under high pressures, (R3) and (R2) are prevalent.

2. ADN COMBUSTION

Combustion of the ADN propellant features a large heat release in the condensed phase, weak thermal feedback with the gas phase, and low burning surface temperature. Most of the research has been focused on combustion of pure ADN pellets, ADN/binder sandwiches, and ADN-based composite propellants. Results obtained have provided good insight into ADN combustion.

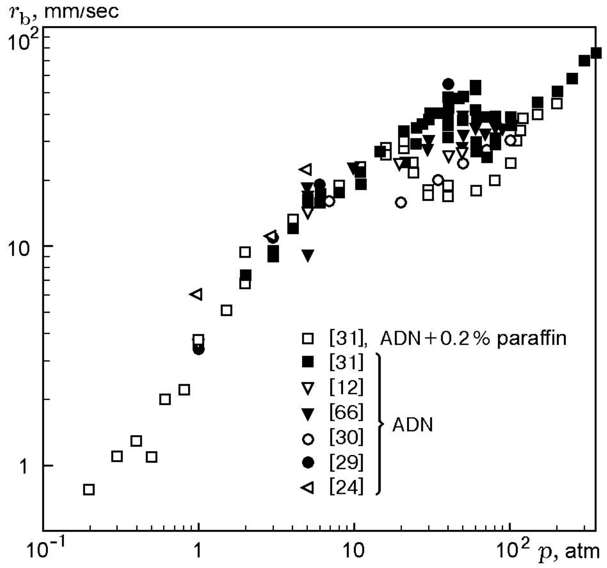

Fig. 1. Pressure sensitivity of the ADN burning rate.

2.1. Overall Combustion Characteristics

The burning rate of ADN below 100 atm [34, 65] is higher than that of other energetic materials, such as CL-20, hydrazinium nitroformate (HNF), HMX, RDX, AP, AN, glycidyl azide polymer (GAP), and *bis*-azido methyl oxetane (BAMO). The calculated flame temperatures of ADN-based composite propellants are close to those of AP-based composite propellants [65], but ADN differs from AP in terms of the relationship between the burning rate and oxidizer dispersion. With increasing particle size, the burning rate of ADN-based propellants increases, whereas the burning rate of AP-based propellants decreases [11]. Figure 1 shows the variation of the burning rate with pressure for pellets made of pure ADN and ADN + 0.2% paraffin [12, 24, 29–31, 66]. Reasonably good agreement between various data sets was obtained in spite of the differences in propellant samples and experimental techniques. At low pressures (1–3 atm), ADN pellets burned non-luminously and the burning rate was $r_b = 3.5$–11 mm/sec [12, 24, 29, 31]. Laser-assisted combustion of ADN pellets at $p = 3$ atm produced an unstable flame with only a weak dependence on the laser heat flux intensity [24]. At $p = 5$–6 atm, pure ADN pellets burned steadily and luminously. Stable combustion of pure ADN first occurred in the pressure range of 5–20 atm and can be described by the empirical relationship $r_b = 20.72p^{0.604}$ [mm/sec] ($p = 0.5$–2.0 MPa). The range of pressures $p = 20$–100 atm is the region of unstable combustion, where the burning rate becomes irregular. The phe-

TABLE 6

ADN Thermal Decomposition Mechanisms

p	T, °C	Mechanisms
10^{-5}, 6 torr	>90	$\mathrm{ADN(s, liq)} \rightarrow \mathrm{ADN(g)} \rightarrow \mathrm{NH_3} + \mathrm{HDN}$ (dominant)
		$\mathrm{HDN} \rightarrow \mathrm{N_2O} + \mathrm{HNO_3}$
		$\mathrm{HDN} \rightarrow \mathrm{NO_2} + \mathrm{HNNO_2}$
		$\mathrm{ADN(s, liq)} \rightarrow \mathrm{ADN(g)} \rightarrow \mathrm{NH_3} + \mathrm{N_2O} + \mathrm{HNO_3}$
1 atm	<92–95	$\mathrm{ADN(s)} \rightarrow \mathrm{N_2O} + \mathrm{NH_4NO_3}$ (dominant)
		$\mathrm{ADN(s)} \rightarrow \mathrm{NO_2} + \mathrm{NH_4NNO_2}$
	95–155	Dominant liquid-phase decomposition:
		$\mathrm{ADN(liq)} \rightarrow \mathrm{N_2O} + \mathrm{NH_4NO_3}$ (competitive)
		$\mathrm{ADN(liq)} \rightarrow \mathrm{NH_3} + \mathrm{N_2O} + \mathrm{HNO_3}$ (competitive)
		Lower gas-phase decomposition:
		$\mathrm{ADN(g)} \rightarrow \mathrm{NH_3} + \mathrm{HDN}$ (competitive)
		$\mathrm{ADN(g)} \rightarrow \mathrm{NH_3} + \mathrm{N_2O} + \mathrm{HNO_3}$ (competitive)
		$\mathrm{HDN} \rightarrow \mathrm{N_2O} + \mathrm{HNO_3}$
		$\mathrm{HDN} \rightarrow \mathrm{NO_2} + \mathrm{HNNO_2}$
		$\mathrm{NH_3} + \mathrm{HNO_3} \rightarrow \mathrm{NH_4NO_3}$ (AN aerosol)
	>155	$\mathrm{ADN(g)} \rightarrow \mathrm{NH_3} + \mathrm{N_2O} + \mathrm{HNO_3}$ (competitive)
		$\mathrm{ADN(g)} \rightarrow \mathrm{NH_3} + \mathrm{HDN}$ (competitive)
		$\mathrm{NH_3} + \mathrm{HNO_3} \rightarrow \mathrm{NH_4NO_3}$ (aerosol)
		$\mathrm{HDN} \rightarrow \mathrm{N_2O} + \mathrm{HNO_3}$
		$\mathrm{HDN} \rightarrow \mathrm{NO_2} + \mathrm{HNNO_2}$
		Major exothermic reactions:
		$\mathrm{NH_3} + \mathrm{NO_2} \rightarrow \mathrm{N_2O} + \mathrm{NO} + \mathrm{N_2} + \mathrm{H_2O}$
		$\mathrm{HNO_3} \rightarrow \mathrm{NO_2} + \mathrm{H_2O} + \mathrm{O_2}$
		$\mathrm{AN(liq)} \rightarrow \mathrm{N_2O} + \mathrm{H_2O}$
>2.0 GPa	120–140	$\mathrm{ADN(s)} \rightarrow \mathrm{N_2O} + \mathrm{NH_4NO_3}$

nomenon may be attributed to the competitive influence between condensed-phase and gas-phase exothermic reactions in determining the propellant surface conditions and the associated burning rate. At high pressures (above 100 atm), stable ADN combustion was observed, which can be described by the expression $r_\mathrm{b} = 8.50p^{0.608}$ [mm/sec] ($p = 10$–36 MPa). Addition of 0.2% of paraffin did not change the burning behavior at low (0.2–20 atm) and high (above 100 atm) pressures. It tended, however, to stabilize combustion in the range of 20–100 atm and ensured a negative dependence of the burning rate on pressure.

The burning rate of pure ADN is very sensitive to its preconditioned temperature [31]. Such a high temperature sensitivity is an important characteristic of ADN combustion. The burning rate of pure ADN also exhibits a relatively high pressure sensitivity in the range of pressures that ensure stable combustion. Price et al. [30] conducted a series of experiments on ADN and its composites with polybutadiene acrylic acid acrylonitrile (PBAN), Al powder, AP, and $\mathrm{Fe_2O_3}$. The propellant samples included: (a) laminae of pressed ADN, ADN + Al, and ADN + $\mathrm{Fe_2O_3}$; (b) sandwiches of ADN/PBAN and ADN/matrix {ADN (or AP) + PBAN}; (c) PBAN/ADN and PBAN/ADN/AP propellants. The PBAN binder consisted of 64.14% of the PBAN pre-polymer, 20.86% of the epoxy curing agent (ECA) and 15.00% of dioctyl adipate (DOA). The burning rates of these samples were measured in the pressure range of 7–105 atm. The following facts were observed.

1) The burning rate of pressed ADN laminae was dependent on the ADN grain size (30 and 350 μm). Pressed ADN/Al laminae had a higher burning rate than ADN laminae. Moreover, the ultrafine Fe_2O_3 powder did not increase the burning rate.

2) The ADN/PBAN sandwich had a higher burning rate than ADN laminae and a pressure sensitivity similar to that of ADN laminae. The burning-rate properties of ADN/matrix {ADN (or AP) + PBAN} sandwich were similar to those of the ADN/PBAN sandwich.

3) PBAN/ADN and PBAN/ADN/AP propellants had relatively lower burning rates at low pressures but a higher sensitivity to pressure than ADN laminae and ADN/PBAN sandwiches.

According to Korobeinichev et al. [67–70], ADN/HTPB (hydroxyl-terminated polybutadiene), ADN/GAP, and ADN/PCL (polycaprolactone) composite propellants burned steadily and luminously, even at 1 atm. Catalysts such as CuO and PbO could eliminate irregular combustion of ADN or maintain the mesa-combustion effect (negative dependence on pressure). Investigations of Parr and Hanson-Parr [71–73] on diffusion flame structures of ADN/binder sandwiches indicated that the burning rates were controlled by ADN. ADN burned rapidly and appeared to leave the non-energetic binder (HTPB or wax) behind. For sandwiches with energetic binders [i.e., GAP or BAMO/NMMO (nitromethyl methyl oxetane)], only small amounts of the fuel (binder) was recovered after the test, implying that the effect of the ADN particle size on the burning rate is possibly negative or non-existent, in contrast to AP. At low pressures ($p < 2$–3 atm), the diffusion flames between ADN and the binder were clearly evident, but the flames became weak or non-existent at elevated pressures.

Many organic amine salts of dinitramide have combustion characteristics similar to those of ADN [10]. Benzylamine and ethanolamine dinitramide salts of high amine basicity showed a region of unstable combustion in the r_b–p coordinates. Most of the amine salts of dinitramide, such as ethylenediamine and aminoguanidine, regardless of their basicity, show a transition region characterized by a reduced exponent in the burning-rate correlation. Some dinitramide salts of minimal basicity demonstrate stable combustion and a constant exponent in the combustion law throughout the entire pressure region. At lower pressures, the burning rate of dinitramide salts decreases with decreasing amine basicity.

In an effort to study the combustion-wave structure, Fetherolf and Litzinger [24] measured the temporal and spatial variations of the temperature field of ADN pellet burning at $p = 5$ atm under laser heating. The temperature in the condensed phase rose almost linearly up to 87°C (near the ADN melting point) and then reached 145°C (corresponding to the onset of rapid pyrolysis of ADN). It finally increased rapidly to ≈400°C (temperature of the ADN burning surface), followed by a gas-phase preparation zone at ≈557°C. The final flame temperature was 1170°C. The measured temperature field was smooth in the condensed phase and the near-surface zone, while it displayed pulsations in the gas phase [12]. Figure 2 shows the temperature profiles measured in [12, 29, 31]. It is clear that the temperature profile in the gas-phase region exhibits a multiple-stage structure dependent on pressure [12]. The burning ADN propellant had a relatively low surface temperature of 280–340°C ($p = 1$–3 atm) or 340–400°C ($p = 5$–10) atm [12, 24, 31]; this temperature increased with increasing pressure. Endothermic dissociation of AN might be responsible for the low surface temperature in ADN combustion.

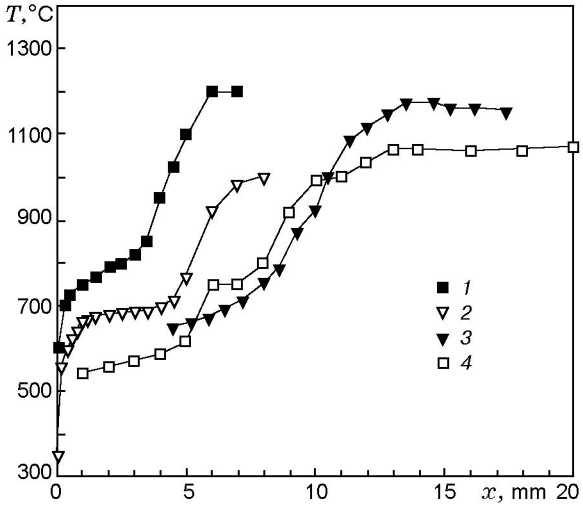

Fig. 2. Temperature profiles for ADN combustion: x is the distance from the burning surface; 1) data of [12] for 10 atm, 20°C, $r_b = 18$ mm/sec, and $\rho = 1.6$ g/cm^3; 2) data of [12] for 5 atm, 20°C, $r_b = 15$ mm/sec, and $\rho = 1.6$ g/cm^3; 3) data of [29] for 6 atm, $r_b = 17.3$ mm/sec, and $\rho = 1.79$ g/cm^3; 4) data of [31] for 5 atm, $r_b = 16$ mm/sec, and $\rho = 1.6$ g/cm^3.

In the pressure range of 5–40 atm, a dark-zone temperature plateau was observed at $T = 600$–1000°C [31]. At $p = 20$ atm, it was observed in the ranges of 570–620°C [31] and 900–1000°C [12]. With increasing pressure, the temperature of the dark zone increased, and its width decreased. At $p < 40$ atm, the final flame temperature was below 1600°C and increased with increasing pressure. At $p = 60$ atm, the final flame tem-

TABLE 7

Temperature Parameters in the ADN Combustion Wave

Parameters	Pressure, atm									
	1	3	5	6	10	20	30	40	60	Reference
T_{f},°C	—	≈1050	1000	—	1200	1400	1580	1700	1800	[12]
		—	≈800	—	≈1010	≈1010	—	≈1240	—	[31]
		—	—	≈1080	—	—	—	≈1700	—	[29]
		—	≈1120	—	—	—	—	—	—	[24]
T_{s},°C	280	—	340	—	345	355	362	368	370	[12]
	300	≈400	—		—	—	—	—	—	[24]
T_{d},°C	450	—	700	—	800	950	1050	1200	—	[12]
	450	—	≈545		≈580	≈620	—	≈780		[31]
	≈370	540	—		—	—	—	—		[29]
	427	≈550	—		—	—	—	—		[24]

perature was ≈1800°C, and there was no dark-zone temperature plateau. The propellant-surface T_{s}, dark-zone T_{d}, and final flame T_{f} temperatures are summarized in Table 7.

The main products of ADN combustion at $p = 3$–6 atm were H_2O, N_2, NO, N_2O, and to a smaller extent, NH_3 and O_2 [24, 29, 66, 68]. AN particles were no longer visible in the luminous flame, and Brill et al. [21] assumed that the presence of the flame eliminated formation of the AN aerosol [21]. On the other hand, Weiser et al. [66] observed continuous infrared radiation of solid particles in the gas phase close to the propellant surface at $p = 50$ atm. In the solid residue of ADN combustion, a considerable amount of AN was detected and reached nearly 100% at 6 atm [31]. For the sample consisting of ADN + 0.2% paraffin, the ratios of the unreacted ADN to AN in the residue were 30/70 at $p = 0.25$ atm, 6/94 at $p = 1$ atm, and less than 1/99 at $p = 6$ atm.

2.2. Combustion Mechanisms

The combustion-wave structure of ADN consists of a condensed-phase and a gas-phase reaction zone. The condensed phase mainly contains melted ADN and AN, part of which is brought into the gas phase near the surface as liquid droplets [31]. The first flame zone can be subdivided into two stages. The first stage involves the dissociation of small AN droplets and the second stage the dissociation of small ADN droplets. Dissociation of small ADN droplets requires a higher temperature than dissociation of small AN droplets, due to stronger acidity of $HN(NO_2)_2$ than HNO_3. The estimated heat of dissociation for ADN is $\Delta H^0_{\mathrm{diss}} = 45$ kcal/mole. After complete consumption of ADN liquid droplets, the second flame begins to form. Considering the first flame temperature to be the dissociation temperature of ADN droplets, Fogelzang et al. [31] obtained a relationship between the pressure and dissociation temperature of ADN:

$$\log(p^*) = -\frac{4929.6}{T} + 6.9 \quad [p^* \text{ in atm; } T \text{ in K}]. \tag{1}$$

In experiments employing a two-temperature flow reactor under vacuum (6 torr), Korobeinichev et al. [29] observed significant ADN deposition at the reactor exit, which serves as evidence for ADN sublimation. They suggested that ADN sublimation and the subsequent decomposition reaction ADN(g) + M → $NH_3 + HN(NO_2)_2$ + M are the dominant initial processes. The sublimation heat for ADN was given as $\Delta H^0_{\mathrm{subl}} = 40$ kcal/mole. The ADN vapor pressure in the reactor (p^*) is described by the equation

$$\log(p^*) = 19.58 - \frac{8.77 \cdot 10^{-3}}{T} \quad [p^* \text{ in torr; } T \text{ in K}]. \tag{2}$$

Zenin et al. [12] presented an ADN burning law

$$m = 13.6 \cdot 10^6 \exp\left(\frac{-38{,}000}{2RT_s}\right) \tag{3}$$

and the rate constant of the solid-phase reactions

$$K = 5 \cdot 10^{17} \exp\left(\frac{-38{,}000}{RT_{\mathrm{s}}}\right) \text{ sec}^{-1} \text{ (1–60 atm)}, \tag{4}$$

where m is the mass burning rate [in g/(cm$^2\cdot$sec)] and T_{s} is the surface temperature (in K); the activation energy is 38 kcal/mole.

Yang et al. [74] suggested the reaction

$$\mathrm{ADN} \rightarrow NH_3 + HNNO_2 + NO_2 \tag{R11}$$

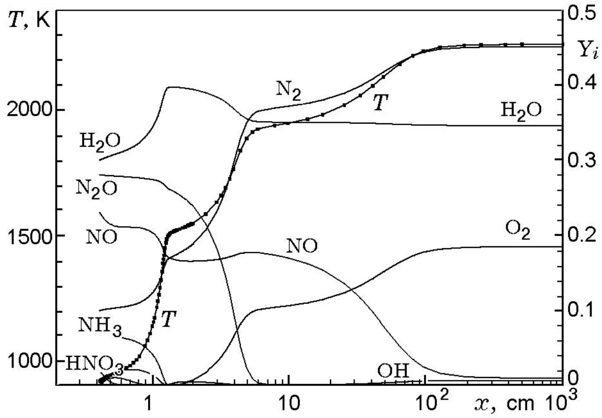

Fig. 3. Predicted profiles of temperature and species concentrations in the ADN flame for $p = 6$ atm [32].

as the initial ADN-decomposition mechanism followed by $HNNO_2$ pyrolysis as in the reaction

$$HNNO_2 \to OH + N_2O. \qquad (R12)$$

Thus, the oxidizing gases near the surface were NO_2, N_2O, and $HNNO_2$, and the reducing gas was NH_3.

A relation between the burning rate and pressure for ADN combustion was formulated by Yang et al. [74] based on their theoretical model:

$$r_b = \frac{1.709p\theta_0(p)}{\rho} \text{ [cm/sec]}, \qquad (5)$$

$$\theta_0(p) = \frac{1 + q_a}{1 + \alpha + \beta + \gamma + q\eta(p) - q_a g(p)}. \qquad (6)$$

Here $\theta_0(p)$ is the mole fraction of the oxidizing gas near the burning surface, p is the pressure (in MPa), ρ is the monopropellant density (in g/cm^3), α, β, γ, q, and q_a are the chemical composition parameters calculated near the surface, and $\eta(p)$ and $g(p)$ are empirical functions [75], which were not provided for ADN.

Liau and Yang [32] and Korobeinichev et al. [68] conducted a detailed numerical investigation of ADN combustion. Based on a kinetic model with 33 species and 180 reactions and the initial step ADN(g) + M $\to NH_3 + HN(NO_2)_2 + M$, the calculated temperature and species concentration profiles [32] at $p = 6$ atm were in good agreement with experimental results, as is shown in Fig. 3. It was found that the oxidation reactions of NH_3, NH_2, and HONO are important in the first flame zone. For the reaction $NH_3 + OH = NH_2 + H_2O$, a 1% increase in the reaction rate could result in a 1.8% increase in temperature, 0.95% increase in H_2O, 27% decrease in NH_3, and 0.37% decrease in N_2O. The experimental and numerical results imply possible changes in the initial decomposition mechanisms with varying pressure.

2.3. Dark Zones in ADN Combustion

According to the experimental results of Zenin et al. [12] and Fogelzang et al. [31] and the numerical investigation by Liau et al. [32], for ADN combustion at $p = 5$–20 atm, the combustion-wave structure exhibits two temperature plateaus, one at 600–1000°C and the other at 1000–1400°C (see Figs. 2 and 3). The temperature plateau at 600–1000°C is referred to as the first dark-zone temperature plateau. Since ADN combustion was completed in the range of the secondary-flame temperature (1000–1400°C) and did not reach its theoretical final flame temperature of ≈1800°C (at $p = 60$ atm), the temperature plateau at 1000–1400°C in the pressure range of 5–20 atm is referred to as the second dark-zone temperature plateau. The lower final flame temperature observed by Zenin et al. [12] in the $p = 5$–20 atm range could possibly be due to heat losses to the ambient medium during the experiments.

The temperature range of the second dark-zone temperature plateau is similar to that of double-base (DB) and nitramine propellants (1200–1600K) [76–79]. The dark-zone characteristics of DB and nitramine propellants are attributed to the low reactivity of NO, CO, and HCN. The species compositions in the dark zone of ADN combustion are listed in Table 8. The high NO mole fraction in the dark zone of the ADN flame is similar to that of DB and nitramine propellants. A high concentration of N_2O is also detected.

In the primary flame zone of ADN combustion, the main reactions are NH_x+NO_x, which significantly affect the chemistry of combustion and the dark-zone parameters. The NH_3 + NO_x reactions have been well studied over the past decades [80–89]. It was found that the species-concentration profiles in the reaction system NH_3 + NO_2 exhibit two different regions with increasing reaction temperature [84, 89]. Below 660°C, the concentrations of NH_3 and NO_2 decreased quickly, while those of NO and N_2O increased rapidly with increasing temperature. For $T > 660$°C, variations in the species concentrations appeared to diminish, and there seemed to be a plateau region for the NO concentration. NO_x reduction by NH_3 was most sensitive to NH_2 radicals. NO produced by the reaction between NH_3 and NO_2 has a tendency to inhibit the reaction system by destroying NH_2 radicals and forming stable N_2 and H_2O species [80–83]. Thus, NO accumulation may cause the reduction of NH_2 radicals and affect the propagation of chain reactions. The experimental data of Bedford and Thomas [82] and the calculations by Thaxton et al. [83] showed that addition of NO significantly decreased the rate of NO_2 decay.

TABLE 8

Species Mole Fractions in the Dark Zones of ADN Combustion

NO	NH_3	N_2	H_2O	N_2O	HNO_2	NO_2	HNO_3	O_2	Note	Reference
0.26	0.012	0.1	0.42	0.22	—	—	0	—	2nd dark zone 6 atm, $L_d = 14$ mm, $T_d = 1460$ K (measured)	[29]
0.17	0	0.17	0.40	0.26	—	—	0	—	2nd dark zone 6 atm, $L_d = 14$ mm, $T_d = 1510$ K (modeling)	[32]
0.16	0.07	0.08	0.31	0.25	0.03	0.03	0.08	—	1st dark zone 3 atm, $L_d = 2$ mm, $T_d = 815$ K (measured)	[68]
0.143	0.10	0.085	0.29	0.235	—	—	0.075	—	1st dark zone 3 atm, $L_d = 2$ mm, $T_d = 785$ K (modeling)	[68]
0.191	0.003	0.155	0.435	0.179	—	—	—	0.019	2nd dark zone 3 atm, $T_d = 1328$ K, laser, $q = 100$ W/cm^2	[24]
0.162	0.012	0.169	0.435	0.184	—	—	—	0.019	2nd dark zone 5 atm, $T_d = 1385$ K, laser, $q = 200$ W/cm^2	[24]

Note. L_d is the flame-standoff distance and T_d the temperature of the dark-zone plateau.

The major reactions in the $NH_3 + NO_2$ system are presented below:

$$NH_3 + NO_2 = NH_2 + HNO, \tag{R13}$$

$$\Delta H_{289\ K} = 103.34\ kJ/mole;$$

$$NH_2 + NO_2 = NH + HNO_2, \tag{R14}$$

$$\Delta H_{289\ K} = 56.48\ kJ/mole;$$

$$NH_2 + NO_2 = N_2O + H_2O, \tag{R15}$$

$$\Delta H_{289\ K} = -361.0\ kJ/mole;$$

$$NH_2 + NO_2 = NO + H_2NO; \tag{R16}$$

$$NH + NO_2 = HNO + NO, \tag{R17}$$

$$\Delta H_{289\ K} = -180.74\ kJ/mole;$$

$$2HNO = H_2O + N_2O, \tag{R18}$$

$$\Delta H_{289\ K} = -342.25\ kJ/mole;$$

$$NH_2 + NO = N_2 + H_2O, \tag{R19}$$

$$\Delta H_{289\ K} = -497.0\ \ kJ/mole;$$

$$NH_2 + NO = N_2H + OH; \tag{R20}$$

$$2HNO_2 = NO_2 + NO + H_2O, \tag{R21}$$

$$\Delta H_{0\ K} = 32.19\ kJ/mole;$$

$$HNO_2 + M = OH + NO + M, \tag{R22}$$

$$\Delta H_{289\ K} = 209\ \ kJ/mole\ [22];$$

$$HNO_2 + OH = NO_2 + H_2O. \tag{R23}$$

Reaction (R13) is considered as a sensitive initial step, and the branching ratio of (R19) to (R20), defined as the ratio of the two reaction rates, is critical. Reaction (R19) consumes NH_2 radicals to produce stable N_2 and H_2O, whereas (R20) consumes NH_2 to produce OH radicals. Consequently, (R19) inhibits the chain reaction, in contrast to the propagation effect of (R20). According to Park and Lin [85–87], the branching ratio between (R19) and (R20) was 0.9/0.1 at $T = 300$ K and 0.78/0.28 at $T = 1000$ K, respectively. Above 1000 K, the ratio sharply decreased with increasing temperature.

Lin and Park showed in their study of gaseous products of ADN decomposition [33] that the concentrations of N_2O and H_2O increased rapidly while NH_3 decreased with increasing temperature. Above 520°C, however, the species concentrations seemed to reach a steady region. This temperature was close to the first dark-zone temperature plateau of ADN combustion. At $p = 6$ atm, the main gas-phase species of ADN combustion products were H_2O (>30%), N_2O (≈30%), NO (25%), and $NH_3 + HNO_3$ (10%) at a distance of about 4 mm from the propellant surface [29]. The existence of $NH_3 + HNO_3$ may be attributed to the inhibition effect of NO. Under these conditions, N_2O is also less reactive. The secondary flame causes the complete consumption of NH_3 and NO_2 or HNO_3 in the system. At the end of the secondary flame, the concentrations of NH_3, NO_2, and HNO_3 almost vanish, but the concentrations of NO and N_2O remain high. The less reactive NO and N_2O at 1000–1400°C contribute to the existence of the second dark-zone temperature plateau. The total rate constant for $NH_2 + NO_2$ in reactions (R14)–(R16) has a negative temperature dependence and is possibly not a critical reaction in ADN combustion. Reactions (R21)–(R23) of HNO_2 should have some influence on the reaction process of ADN.

The first dark-zone temperature is known to increase with pressure (see Fig. 2). A possible reason is that the branching ratio of reactions (R19) and (R20) decreases with increasing pressure, chain development is enhanced, and the primary flame temperature increases. If the pressure is sufficiently high, reaction (20) completely dominates, chain reactions are not inhibited, and the dark-zone temperature plateau is not formed.

The species concentration profiles measured by Korobeinichev et al. [68] indicated that H_2O increased rapidly at approximately 6 mm from the propellant surface, and NO increased slightly, whereas $NH_3 + HNO_3$ and N_2O decreased. At about 12 mm, the H_2O, NO, and N_2O mole fractions were constant at about 45, 25, and 20%, respectively, $NH_3 + HNO_3$ was nearly zero, and the N_2 mole fraction was also constant. On the other hand, the numerical calculations by Liau et al. [32] and Korobeinichev et al. [68] indicated that the mole fractions of NO and NH_3 decreased rapidly at a distance of 8–10 mm from the propellant surface, while those of H_2O and N_2 increased rapidly, and the N_2O concentration was nearly constant. Owing to rapid consumption of NO, its concentration leveled off in the second dark zone. Since the species in this region are mainly NO, N_2O, N_2, and H_2O, it is reasonable to assume that the second dark zone behaves in a manner similar to that for DB and nitramine propellants.

Using a detailed gas-phase chemical-kinetics model consisting of 33 species and 180 reactions, Liau et al. [32] performed a numerical analysis on the sensitivity of temperature and species-concentrations in ADN combustion. The sensitivity coefficient is defined as

$$S_{ij}(x) = \frac{\partial(\ln X_i)}{\partial(\ln A_j)}, \qquad (7)$$

where X_i is the temperature or the mole fraction of the ith species, A_j is the kinetic prefactor of the jth reaction, and x is the distance from the propellant surface. It was found that reactions (R20) and (R19) had a positive and a negative effect, respectively, on the gas-phase temperature, and $\partial(\ln T)/\partial(\ln A)$ reached a maximum value at 11 mm from the surface. On the contrary, the effect of reaction (R19) on the NH_3 concentration was positive, whereas the effect of reaction (R20) was negative, and $\partial(\ln NH_3)/\partial(\ln A)$ had a maximum at 12 mm from the surface, as is shown in Fig. 4. Reaction (R19) producing H_2O showed a negative effect on the H_2O concentration, whereas the effect of reaction (R20) was positive. It was noted that the maximum of $S_{ij}(x)$ was located at a distance of 11–12 mm from the propellant surface, a position slightly downstream of the secondary flame.

2.4. Combustion Irregularity

ADN combustion is stable in the pressure range of 5–20 atm but becomes irregular in the range of 20–100 atm, as is shown in Fig. 1. A further increase in pressure to 100 atm and above produces a stabilizing effect on ADN combustion. Sinditskii et al. [10] and Fogelzang et al. [31] found that other dinitramide salts displayed combustion characteristics analogous to those of ADN. At low pressures, decomposition of dinitramide salts in the condensed phase is maintained by heat released during formation of the ammonium nitrate and N_2O (e.g., ADN → AN + N_2O). This process dictates the burning rate of ADN, since the heat feedback from the gas phase to the propellant surface accounts for a small fraction of energy required to pyrolyze

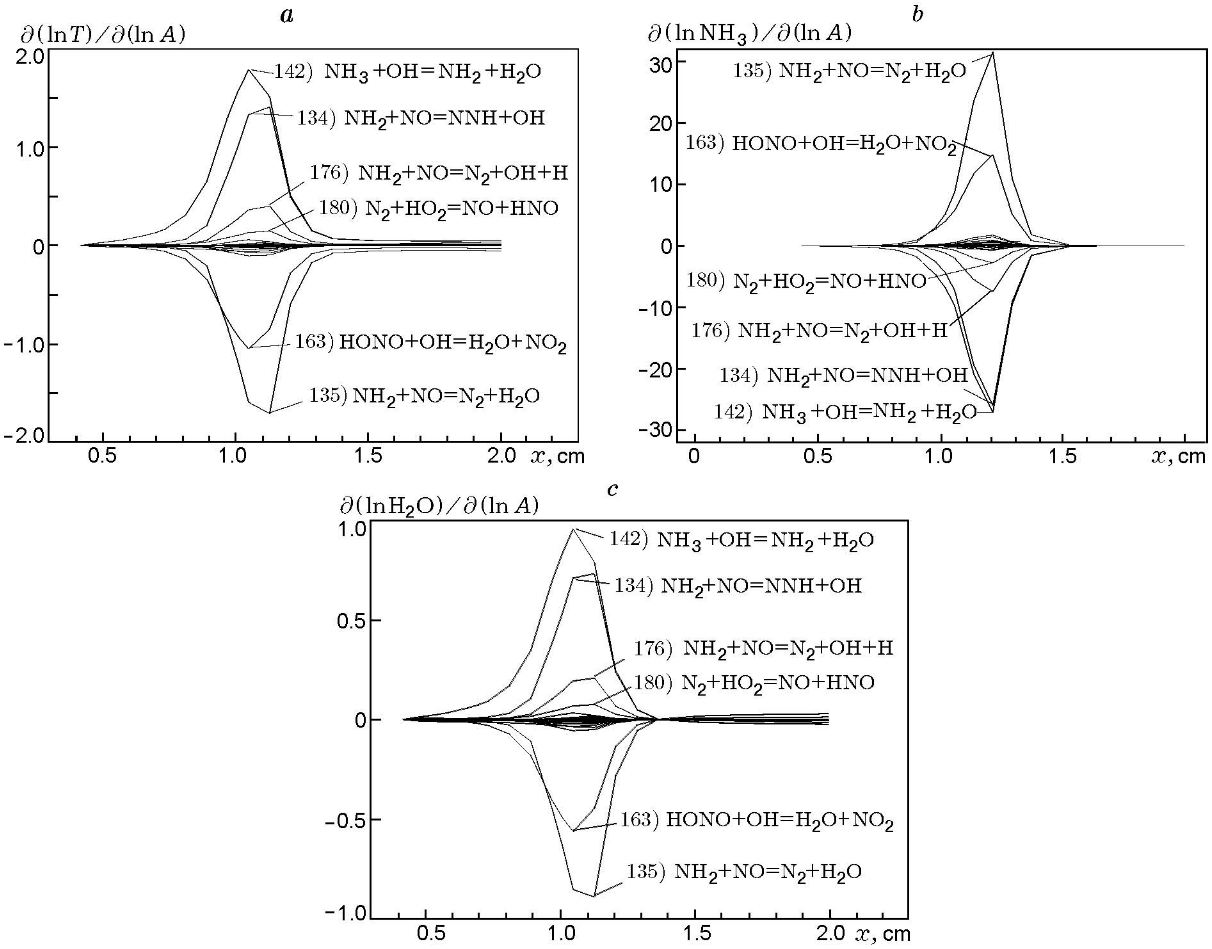

Fig. 4. Normalized sensitivity coefficients of temperature [32] (a), NH_3 concentration [32] (b), and H_2O concentration [32] (c).

the condensed-phase ADN. As the pressure increases, the extent of ejection and entrainment of molten ADN into the gas phase is suppressed. Consequently, the net amount of heat release in the condensed phase and the surface temperature increase, resulting in a higher burning rate. The gas-phase reactions become more intense, which is evidenced by enhanced flame luminosity at higher pressures, and the primary flame is firmly established near the propellant surface when the pressure exceeds 5 atm. The resultant energy transfer to the condensed phase, though still weak as compared with the condensed-phase exothermic reactions for $p < 20$ atm, plays a noticeable role in determining the energy balance at the propellant surface and in the subsurface region. As the pressure reaches ≈100 atm and above, the secondary flame merges into the primary flame. Rapid enhancement of heat release in the gas phase immediately above the propellant surface and its ensuing energy transfer to the condensed phase dictate the propellant burning behavior. The influence of hydrodynamic and rheologic instabilities in the melt layer essentially disappears. The absence of a two-phase mixture in the subsurface region and the change in the morphological structure may be responsible for the sudden decrease in the burning rate at a pressure of ≈ 100 atm.

Based on the solid residue collected from the ADN combustion experiment, Fogelzang et al. [31] inferred that the AN content was more than 99% at $p = 6$ atm. The ADN crystal could not burn regularly in the range $p = 20$–100 atm. Instead, it cracked down and decomposed to form solid AN particles. The AN decomposition rate, however, could not keep up with the cracking rate. The irregular combustion behavior of ADN could, thus, be correlated to the formation of a massive amount of AN on the ADN burning surface. At lower pressures, the ADN crystal particles first undergo melting to form a surface liquid layer, followed by thermal decomposition and even vaporization. The solid-phase decomposition of the ADN crystal is less intense, and thus cracking of the ADN crystal does not occur at lower pressures.

With increasing pressure, the liquid layer at the propellant surface becomes thinner, and the condensed-phase decomposition of ADN particles to AN + N_2O is reduced. Owing to its low burning rate, the abundance of pure AN at the propellant surface is disadvantageous to the burning rate of ADN. In contrast, cracking of the ADN crystal to form solid AN particles can be advantageous, since the process increases the effective surface area for heat transfer. These two conflicting factors contribute to the irregular changes in the burning rate of ADN in the pressure range of 20–100 atm.

For high pressures ($p > 100$ atm), the gas-phase heat release and feedback become significant. The resultant higher surface temperature accelerates decomposition. The AN dissociation rate can keep up with the solid-phase decomposition of ADN. The effect of the ADN particle size on the burning rate can be attributed to the solid-phase decomposition mechanism, where larger ADN particles produce more cracks and higher porosity and, hence, a higher burning rate.

CONCLUSIONS

ADN thermal decomposition mechanisms depend strongly on pressure, preconditioned temperature, and experimental techniques. Decomposition is acid-catalytic and self-accelerated, but retarded by water and bases. The major characteristics include an irregular DSC exothermic peak, formation of massive amounts of AN and N_2O due to solid-phase dissociation, and a two-stage decomposition process exhibiting high and low activation energies above and below 160°C, respectively. The lower activation energy (<30 kcal/mole) can possibly be attributed to condensed-phase dissociation of ADN, and the higher activation energy (about 40 kcal/mole) to gas-phase dissociation of ADN.

Below the melting point, in the solid phase, ADN decomposes in accordance with the mechanism ADN $\rightarrow NH_4NO_3 + N_2O$, which may occur through a pathway of multimolecular rearrangement. Liquid-phase decomposition of ADN may take place through one of the two competing mechanisms, ADN $\rightarrow NH_4NO_3+N_2O$ or ADN $\rightarrow NH_3+HNO_3+N_2O$, while the competing mechanisms in the gas phase are ADN $\rightarrow NH_3$ + HDN and ADN $\rightarrow NH_3+HNO_3+N_2O$. It is difficult in practice to experimentally distinguish ADN = $NH_3+HNO_3+N_2O$ from the series of reactions ADN = NH_3 + HDN followed by HDN = $N_2O + HNO_3$, and to distinguish ADN = AN + N_2O from the series of reactions ADN = NH_3 + HDN followed by HDN = $N_2O + HNO_3$ and $NH_3 + HNO_3$ = AN.

ADN combustion is characterized by intense energy release in the condensed phase, weak heat feedback from the gas phase, and high burning rate. The combustion-wave structure of ADN includes a condensed-phase region, a primary flame followed by a dark-zone temperature plateau, a secondary flame followed by another dark-zone temperature plateau, and a final flame. The flame structure depends strongly on pressure. ADN combustion is stable in the pressure range of 5–20 atm, and the burning rate is controlled by exothermic decomposition reactions in the condensed phase. At pressures of 100 atm and above, the secondary flame merges into the primary flame. The gas phase exhibits a monotonic increase in temperature to 1800°C at the end of the final flame. The intense heat feedback from the gas phase dictates the burning surface condition and is sufficient to support AN dissociation, so that the propellant combustion becomes stable again. In the range of 20–100 atm, combustion irregularity occurs, along with the scatter of the burning-rate data with respect to pressure. The phenomenon may be attributed to the competitive influence of the condensed-phase and gas-phase exothermic reactions in determining the propellant-surface conditions and the associated burning rates. The changes in the gas-phase flame structure, burning-surface rheology, and subsurface morphological structure also exert a significant influence on the burning characteristics.

Experimental research of reaction systems of NH_3 with NO_2, HONO, and HNO_3 for $T = 600$–1000 and 1000–1400°C are critical for understanding the gas-phase flame structure. The first dark-zone temperature plateau (600–1000°C) in ADN combustion at $p = 5$–20 atm results from the inhibition effect of NO in the reaction system of NH_3 and NO_2. The presence of the second dark-zone temperature plateau (1000–1400°C) is attributed to the low reactivity of NO and N_2O.

In spite of the substantial progress achieved to date, there still remain a number of unresolved issues. In particular, a well-grounded theory needs to be established to help understand the irregular burning phenomenon in the pressure range of 20–100 atm. Reaction mechanisms, such as ADN = AN + N_2O and ADN = $NH_3+HNO_3+N_2O$, and propellant thermodynamics and transport over the entire ranges of pressure and preconditioned temperature of concern also require a thorough investigation.

This work was sponsored partly by the Pennsylvania State University, partly by the Beijing Institute of

Technology, partly by the California Institute of Technology Multidisciplinary University Research Initiative under (ONR Grant No. N00014-95-1-1338, and partly by subcontracts from Software Engineering Associates (SEA), Carson City, NV (ONR Contract No. N00014-02-C-0292, Judah Goldwasser as a Contract Monitor).

REFERENCES

1. S. Bormann, "Advanced energetic materials emerge for military and space applications," *Chem. Eng. News*, Jan. 17, 18–22 (1994).
2. J. C. Bottaro, P. E. Penwell, and R. J. Schmitt, "1,1,3,3-Tetraoxo-1,2,3-Triazapropene anion, a new oxy anion of nitrogen: The dinitramide anion and its salts," *J. Amer. Chem. Soc.*, **119**, 9405–9410 (1997).
3. S. Venkatachalam, G. Santhosh, and K. N. Ninan, "An overview on the synthetic routes and properties of ammonium dinitramide (ADN) and other dinitramide salts," *Propel., Expl., Pyrotech.*, **29**, 178–187 (2004).
4. O. A. Lukyanov, O. V. Anikin, V. P. Gorelik, and V. A. Tartakovsky, "Dinitramide and its salts. 3. Metallic salts of dinitramide," *Russ. Chem. Bull.*, **43**, 1457–1461 (1994).
5. O. A. Lukyanov, A. R. Agevnin, A. A. Leichenko, et al., "Dinitramide and its salts. 6. Dinitramide salts derived from ammonium bases," *Russ. Chem. Bull.*, **44**, 108–112 (1995).
6. R. D. Gilardi, J. Flippen-Anderson, C. George, and R. J. Buther, "A new class of flexible energetic salts: the crystal structures of the ammonium, lithium, potassium, and cesium salts of dinitramide," *J. Amer. Chem. Soc.*, **119**, 9411–9416 (1997).
7. R. D. Gilardi and R. J. Butcher, "A new class of flexible energetic salts. Part 4: The crystal structures of hexaaquomagnesium (II), hexaaquomanganese (II), and hexaaquozinc (II) dihydrate salts of dinitramide," *J. Chem. Crystallogr.*, **28**, 105–110 (1998).
8. R. J. Butcher and R. D. Gilardi, "A new class of flexible energetic salts. Part 2: The crystal structures of the cubane-1,4-diammonium dinitramide and cubane-1,2,4,7-tetraammonium dinitramide salts," *ibid.*, pp. 95–104.
9. R. D. Gilardi and R. J. Butcher, "A new class of flexible energetic salts. Part 3: The crystal structures of the 3,3-dinitroazetidinium dinitramide and 1-i-propyl-3,3-dinitroazetidinium dinitramide salts," *ibid.*, pp. 163–169.
10. V. P. Sinditskii, A. E. Fogelzang, A. I. Levshenkov, et al., "Combustion behavior of dinitramide salts," AIAA Paper No. 98-0808 (1998).
11. Z. Pak, "Some ways to higher environmental safety of solid rocket propellant application," AIAA Paper No. 93-1755 (1993).
12. A. A. Zenin, V. M. Puchkov, and S. V. Finjakov, "Physics of ADN combustion," AIAA Paper No. 99-0595 (1999).
13. R. J. Schmitt, J. C. Bottaro, and P. E. Penwell, "Synthesis of cubane based energetic molecules," AD-A 263271 (1993).
14. T. P. Russell, G. J. Piermari, S. Block, and P. J. Miller, "Pressure, temperature reaction phase diagram for ammonium dinitramide," *J. Phys. Chem.*, **100**, 3248–3251 (1996).
15. T. P. Russell, A. G. Stern, W. M. Koppes, and C. D. Bedford, "Thermal decomposition and stabilization of ammonium dinitramide," in: *Proc. 29th JANNAF Combustion Subcommittee Meeting*, CPIA Publ. No. 593, Vol. II (1992), pp. 339–345.
16. M. D. Pace, "Spin trapping of nitrogen dioxide from photolysis of sodium nitrite, ammonium nitrate, ammonium dinitramide, and cyclic nitramines," *J. Phys. Chem.*, **98**, 6251–6257 (1994).
17. V. A. Shlyapochnikov, G. I. Oleneva, N. O. Cherskaya, et al., "Molecular absorption spectra of dinitramide and its salts," *J. Mol. Struct.*, **348**, 103–106 (1995).
18. V. A. Shlyapochnikov, N. O. Cherskaya, O. A. Luk'yanov, et al., "Dinitramide and its salts. 4. Molecular structure of dinitramide," *Russ. Chem. Bull.*, **43**, 1522–1525 (1994).
19. V. A. Shlyapochnikov, G. I. Oleneva, N. O. Cherskaya, et al., "Dinitramide and its salts," *Russ. Chem. Bull.*, **44**, 1449–1453 (1995).
20. K. O. Christe, W. W. Wilson, M. A. Petrie, et al., "The dinitramide anion, $N(NO_2)_2$," *Inorg. Chem.*, **35**, 5068–5071 (1996).
21. T. B. Brill, P. J. Brush, and D. G. Patil, "Thermal decomposition of energetic materials 58. Chemistry of ammonium nitrate and ammonium dinitramide near the burning surface temperature," *Combust. Flame*, **92**, 178–186 (1993).
22. P. Politzer, J. M. Seminario, and M. C. Concha, "Energetics of ammonium dinitramide decomposition steps," *J. Mol. Struct.* (*Theochem.*), **427**, 123–129 (1998).
23. A. M. Mebel, M. C. Lin, K. Morokuma, et al., "Theoretical study of the gas-phase structure, thermochemistry, and decomposition mechanisms of NH_4NO_2 and $NH_4N(NO_2)$," *J. Phys. Chem.*, **99**, 6842–6848 (1995).
24. B. L. Fetherolf and T. A. Litzinger, "CO_2 laser-induced combustion of ammonium dinitramide (ADN)," *Combust. Flame*, **114**, 515–530 (1998).
25. M. J. Rossi, J. C. Bottaro, and D. F. McMillen, "The thermal decomposition of the new energetic material ammonium dinitramide ($NH_4N(NO_2)_2$) in relation to nitramide (NH_2NO_2) and NH_4NO_3," *Int. J. Chem. Kinet.*, **25**, 549–570 (1993).
26. S. Lobbecke, H. H. Krause, and A. Pfeil, "Thermal analysis of ammonium dinitramide decomposition," *Propel., Expl., Pyrotech.*, **22**, 184–188 (1997).

27. A. I. Kazakov, Y. I. Rubtsov, and G. B. Manelis, "Kinetics and mechanism of thermal decomposition of dinitramide," *Propel., Expl., Pyrotech.*, **24**, 37–42 (1999).
28. A. S. Tompa, "Thermal analysis of ammonium dinitramide (ADN)," *Thermochim. Acta*, **357–358**, 177–193 (1999).
29. O. P. Korobeinichev, L. V. Kuibida, A. A. Paletsky, et al., "Development and application of molecular beam mass-spectrometry to the study of ADN combustion chemistry," AIAA Paper No. 98-0445 (1998).
30. E. W. Price, S. R. Chakravarthy, J. M. Freeman, et al., "Combustion of propellants with ADN," AIAA Paper No. 98-3387 (1998).
31. A. E. Fogelzang, V. P. Stinditskii, V. Y. Egroshev, et al., "Combustion behavior and flame structure of ammonium dinitramide," in: *Proc. 28th Int. Ann. Conf. ICT*, Karlsruhe, FRG, June 24–27 (1997), pp. 1–14.
32. Y. C. Liau, V. Yang, M. C. Lin, and J. Park, "Analysis of ADN combustion with detailed chemistry," in: *Proc. 35th JANNAF Combustion Subcommittee Meeting*, CPIA Publ. (1998).
33. M. C. Lin and J. Park, "Thermal decomposition of gaseous ammonium dinitramide at low pressure: Kinetic modeling of product formation with *ab initio* MO/VRRKM calculations," in: *Proc. 27th Symp.* (*Int.*) *on the Combustion*, Vol. 2, The Combustion Inst., Pittsburgh (1998), pp. 2351–2357.
34. A. I. Atwood, T. L. Boggs, P. O. Curran, et al., "Burn rate of solid propellant ingredients. Part 1: Pressure and initial temperature effects," *J. Propuls. Power*, **15**, 740–752 (1999).
35. J. C. Oxley, J. L. Smith, W. Zhang, et al., "Thermal decomposition studies on ammonium dinitramide (ADN) and ^{15}N and ^{2}H isotopomers," *J. Phys. Chem.*, **101**, 5646–5652 (1997).
36. S. Vyazovkin and C. Wight, "Ammonium dinitramide: Kinetics and mechanism of thermal decomposition," *ibid.*, pp. 5653–5658.
37. S. Vyazovkin and C. Wight, "Thermal decomposition of ammonium dinitramide at moderate and high temperatures," *ibid.*, pp. 7217–7221.
38. S. Vyazovkin and C. Wight, "Isothermal and non-isothermal reaction kinetics in solids: In search of ways toward consensus," *ibid.*, pp. 8279–8284.
39. A. S. Tompa, R. F. Boswell, P. Skahan, et al., "Low/high temperature relationships in dinitramide salts by DEA/DSC and study of oxidation of aluminum powders by DSC/TG," *J. Therm. Anal.*, **49**, 1161–1170 (1997).
40. H. H. Michels and J. A. Montgomery, Jr., "On the structure and thermochemistry of hydrogen dinitramide," *J. Phys. Chem.*, **97**, 6602–6606 (1993).
41. A. N. Pavlov and G. M. Nazin, "Decomposition mechanisms of dinitramide onium salts," *Russ. Chem. Bull.*, **46**, 1848–1850 (1997).
42. A. Langlet, N. Wingborg, and H. Ostmart, "ADN: A new and promising oxidizer for composite rocket propellants," in: K. K. Kuo (ed.), *Challenges in Propellants and Combustion: 100 Years after Nobel*, Begell House, New York (1997), pp. 616–626.
43. S. B. Babkin, A. N. Pavlov, and G. M. Nazin, "Anomalous decomposition of dinitramide metal salts in the solid phase," *Russ. Chem. Bull.*, **46**, 1844–1847 (1997).
44. F. I. Dubovitskii, G. A. Volkov, V. N. Grebennikov, et al., "Thermal decomposition of potassium dinitramide in the liquid state," *Dokl. Chem.*, **347**, 106–108 (1996).
45. M. L. Chan, A. Turner, L. Merwin, et al., "ADN propellant technology," in: K. K. Kuo (ed.), *Challenges in Propellants and Combustion: 100 Years after Nobel*, Begell House, New York (1997), pp. 627–635.
46. G. B. Manelis, "Thermal decomposition of dinitramide ammonium salt," in: *Proc. 26th Int. Ann. Conf. ICT,* Karlsruhe, FRG, July 4–7 (1995), pp. 15.1–15.17.
47. A. I. Kazakov, Yu. I. Rubtsov, L. P. Andrienko, and G. B. Manelis, "Kinetics of the thermal decomposition of dinitramide. 3. Kinetics of the heat release at ADN thermolysis in the liquid phase," *Russ. Chem. Bull.*, **47**, 379–385 (1998).
48. J. P. Agrawal, S. M. Walley, and J. E. Field, "High-speed photographic study of the impact response of ammonium dinitramide and glycidyl azide polymer," *J. Propuls. Power*, **13**, 463–470 (1997).
49. H. Hatano, T. Onda, K. Shiino, et al., "New scientific methods and properties of ammonium dinitramide," *Kayaku Gakkaishi*, **57**, 160–165 (1996).
50. K. J. Krautle and A. J. Atwood, "The reaction of ammonium dinitramide under thermal load," in: *Proc. 29th JANNAF Combust. Subcommittee Meeting*, CPIA Publ. No. 593, Vol. IV (1992), p. 157.
51. L. Lobbecke, S. Krause, and A. Pfeil, "Thermal decomposition and stabilization of ammonium dinitramide (ADN)," in: *Proc. 28th Int. Ann. Conf. ICT*, Karlsruhe, FRG, June 24–27 (1997), pp. 112.1–112.8.
52. W. A. Rosser, S. H. Inami, and H. Wise, "The kinetics of decomposition of liquid ammonium nitrate," *J. Phys. Chem.*, **67**, 1753–1757 (1963).
53. G. Santhosh, S. Venkatachalam, A. U. Francis, et al., "Thermal decomposition kinetic studies on ammonium dinitramide (ADN)–glycidyl azide polymer (GAP) system," in: *Proc. 33rd Int. Ann. Conf. ICT*, Karlsruhe, FRG, July (2002), pp. 64.1–64.14.
54. J. Hommel and J.-F. Trubert, "Study of the condensed phase degradation and combustion of two new energetic charges for low polluting and smokeless propellants: HNIW and ADN," *ibid.*, pp. 10.1–17.8.

55. P. Politzer and J. M. Seminario, "Computational study of the structure of dinitraminic acid, $HN(NO_2)_2$, and the energetics of some possible decomposition steps," *Chem. Phys. Lett.*, **216**, 348–352 (1993).
56. A. I. Kazakov, Yu. I. Rubtsov, G. B. Manelis, and L. P. Andrienko, "Kinetics of the thermal decomposition of dinitramide. 1. The decomposition of different forms of dinitramide," *Russ. Chem. Bull.*, **46**, 2015–2020 (1997).
57. A. I. Kazakov, Yu. I. Rubtsov, G. B. Manelis, and L. P. Andrienko, "Kinetics of the thermal decomposition of dinitramide. 2. Kinetics of the interaction of dinitramide with the decomposition products and other components of a solution," *Russ. Chem. Bull.*, **47**, 39–44 (1998).
58. R. J. Schmitt, M. Krempp, and V. M. Bierbaum, "Gas phase chemistry of dinitramide and nitroacetylide ions," *Int. J. Mass Spectrom. Ion Proces.*, **117**, 621–632 (1992).
59. P. Politzer, J. M. Serminario, M. C. Concha, and P. C. Redfern, "Density functional study of the structure and some decomposition reactions of the dinitramide anion $N(NO_2)_2$," *J. Mol. Struct.* (*Theochem.*), **287**, 235–240 (1993).
60. R. J. Doyle, Jr., "Sputtered ammonium dinitramide: tandem mass spectrometry of a new ionic nitramine," *Org. Mass Spectrom.*, **28**, 83–91 (1993).
61. G. Ferick, "The dissociation pressure and free energy of formation of ammonium nitrate," *J. Amer. Chem. Soc.*, **76**, 5858–5860 (1954).
62. G. Ferick and R. M. Hainer, "On the thermal decomposition of ammonium nitrate. Steady-state reaction temperatures and reaction rate," *J. Amer. Chem. Soc.*, **76**, 5860–5863 (1954).
63. S. Alavi and D. L. Thompson, "Proton transfer in gas-phase ammonium dinitramide clusters," *J. Chem. Phys.*, **118**, 2599–2605 (2003).
64. M. D. Cliff, M. W. Smith, and D. P. Edwards, "Evidence of nitrate formation from the thermal decay of alkali metal dinitramides," *Propel., Expl., Pyrotech.*, **24**, 43–45 (1999).
65. M. W. Beckstead, "Overview of combustion mechanisms and flame structures for advanced," in: V. Yang, T. B. Brill, and W.-Z. Ren (eds.), *Progress in Astronautics and Aeronautics*, Vol. 185: *Solid Propellants in Solid Propellant Chemistry, Combustion, and Motor Interior Ballistics* (2000), pp. 267–285.
66. V. Weiser, N. Eisenrich, A. Baier, and W. Eckl, "Burning behavior of ADN formulations," *Propel., Expl., Pyrotech.*, **24**, 163–167 (1999).
67. O. P. Korobeinichev and A. A. Paletsky, "Flame structure of ADN/HTPB composite propellants," *Combust. Flame*, **127**, 2059–2065 (2001).
68. O. P. Korobeinichev, T. A. Bolshova, and A. A. Paletsky, "Modeling the chemical reactions of ammonium dinitramide (ADN) in a flame," *Combust. Flame*, **126**, 1516–1523 (2001).
69. L. V. Kuibida, O. P. Korobeinichev, A. G. Shmakov, et al., "Mass spectrometric study of combustion of GAP- and ADN-based propellants," *ibid.*, pp. 1655–1661.
70. O. P. Korobeinichev, A. A. Paletsky, A. G. Tereschenko, and E. N. Volkov, "Study of combustion characteristics of ammonium dinitramide/polycaprolactone propellants," *J. Propuls. Power*, **19**, 203–212 (2003).
71. T. Parr and D. Hanson-Parr, "ADN Propellant Diffusion Flame Structure," in: *Proc. 29th JANNAF Combustion Subcommittee Meeting*, CPIA Publ. No. 593, Vol. II (1992), pp. 313–327.
72. T. Parr and D. Hanson-Parr, "ADN diffusion flame structure at elevated pressure," in: *Proc. 30th JANNAF Combustion Subcommittee Meeting*, CPIA Publ. No. 606, Vol. II (1993), pp. 1–13.
73. T. P. Parr and D. M. Hanson-Parr, "Solid propellant diffusion flame structure," in: *Proc. 26th Symp.* (*Int.*) *on Combustion*, The Combustion Inst., Pittsburgh (1996), pp. 1981–1987.
74. D. Yang, H. Song, F. Zhao, et al., "Theoretical calculation of burning rate characteristics of ADN and its mixtures," *J. Propuls. Technol.* (in Chinese), **19**, 87–91 (1998).
75. D. Yang, H. Song, F. Zhao, and S. Li, "Burning-rate prediction of double-base plateau propellants," in: V. Yang, T. B. Brill, and W.-Z. Ren (eds.), *Progress in Astronautics and Aeronautics*, Vol. 185: *Solid Propellant Chemistry, Combustion, and Motor Interior Ballistics*, (2000), pp. 533–548.
76. N. Kubota, "Survey of rocket propellants and their combustion characteristics," in: K. K. Kuo and M. Summerfield (eds.), *Progress in Astronautics and Aeronautics*, Vol. 90: *Fundamentals of Solid-Propellant Combustion* (1984), pp. 1–52.
77. A. Bizot and M. W. Beckstead, "A model for double base propellant combustion," in: *22nd Symp.* (*Int.*) *on Combustion*, The Combustion Inst., Pittsburgh (1988), pp. 1827–1834.
78. D. Hanson-Parr and T. Parr, "RDX laser assisted flame structure," in: *Proc. 31st JANNAF Combustion Subcommittee Meeting*, CPIA Publ. No. 620, Vol. II (1994), pp. 407–423.
79. Y.-C. Liau and V. Yang, "On the existence of the dark-zone temperature plateau in RDX monopropellant combustion," AIAA Paper No. 97-0589 (1997).
80. W. A. Rosser (Jr.) and H. Wise, "Gas-phase oxidation of ammonia by nitrogen dioxide," *J. Chem. Phys.*, **25**, 1078–1079 (1956).
81. F. Falk and R. N. Pease, "An initial report on the stoichiometry and kinetics of the gas phase reaction of nitrogen dioxide and ammonia," *J. Amer. Chem. Soc.*, **76**, 4746–4747 (1954).

82. G. Bedford and J. H. Thomas, “Reaction between ammonia and nitrogen dioxide,” *JCS Faraday Trans. I*, **68**, 2163–2170 (1972).
83. A. G. Thaxton, C.-C. Hsu, and M. C. Lin, “Rate constant for the $NH_3 + NO_2 \rightarrow NH_2 + HONO$ reaction: Comparison of kinetically modeled and predicted results,” *Int. J. Chem. Kinet.*, **29**, 245–251 (1997).
84. J. Park and M. C. Lin, “Mass-spectrometric determination of product branching probabilities for the $NH_2 + NO_2$ reaction at temperatures between 300 and 990 K,” *Int. J. Chem. Kinet.*, **28**, 879–883 (1996).
85. J. Park and M. C. Lin, “Laser-initiated NO reduction by NH_3: Total rate constant and product branching ratio measurements for the $NH_2 + NO$ reaction,” *J. Phys. Chem. A*, **101**, 5–13 (1997).
86. J. Park and M. C. Lin, “A mass spectrometric study of the $NH_2 + NO_2$ reaction,” *J. Phys. Chem. A*, **101**, 2643–2647 (1997).
87. J. Park and M. C. Lin, “Direct determination of product branching for the $NH_2 + NO$ reaction at temperatures between 302 and 1060 K,” *J. Phys. Chem.*, **100**, 3317–3319 (1996).
88. A. M. Mebel and M. C. Lin, “Reactions of NO with nitrogen hydrides,” *Int. Rev. Phys. Chem.*, **16**, 249–266 (1997).
89. P. Glarborg, Dam-Johansen, J. A. Miller, et al., “Modeling the thermal DENOx process in flow reactors. Surface effects and nitrous oxide formation,” *Int. J. Chem. Kinet.*, **26**, 421–436 (1994).